

Geochemical Constraints of the Ediacaran Volcano-Sedimentary Succession of the Sa'al Metamorphic Complex at Wadi Zaghra, South Sinai, Egypt



Michael S. D. AMUEL, Hilmy MOUSSA E. , Mokhles K. AZER* and Doris S. GHABRIAL

Geological Sciences Department, National Research Centre (NRC), Cairo, Egypt

Abstract: The volcano-sedimentary succession around Wadi Zaghra in Sinai, at the northernmost segment of the Arabian Nubian Shield, comprises volcanic rocks interbedded with rather immature sediments. The succession is dominated by intermediate to silicic volcanics of medium- to high-K calc-alkaline affinity. It is divided into two units, the lower unit includes intermediate rocks and dacites interbedded with graywackes, semi-pelites and pelites and topped by polymict conglomerates. This unit is subjected to folding and regional metamorphism (up to garnet zone) and is intruded by quartz diorite-granodiorite inducing, locally, low-pressure contact thermal metamorphism. The unmetamorphosed upper unit encompasses acid volcanics intercalated with litharenite, sublitharenite and minor arenite. The rhyolites of this unit pertain to the highly fractionated granites and are characterized by an agpaite index (NK/A) ranging from 0.87 to 0.96. They may reflect either extensive interaction of subduction-related magmas with the continental crust or a change in the tectonic regime. The present lithological and geochemical characteristics of the studied sediments together with available zircon ages indicate rather distal provenance of their detritus. This detritus comprises fluvial-alluvial sediments accumulated in the intermontane basins, which are half-grabens or tilted fault blocks. The tectonic setting of the depositional basins is active continental margin and continental island arcs. Geochemical patterns of the Zaghra volcano-sedimentary succession indicate their correlation with the Dokhan Volcanics-Hammamat Clastics sequence of the Eastern Desert of Egypt. Also, the Zaghra volcanics display geochemical similarities with those exposed in Sinai, at the Rutig, Ferani and Iqna Shar'a areas. The Zaghra succession is dated as Ediacaran but is not related either to the ensimatic island arc assemblage or to the rift-related assemblage formed during the early stages of the break-up of Rodinia as previously thought.

Key words: geochemistry, Neoproterozoic, Dokhan Volcanics, Arabian-Nubian Shield, Sinai, Egypt

Citation: Samuel et al., 2019. Geochemical Constraints of the Ediacaran Volcano-Sedimentary Succession of the Sa'al Metamorphic Complex at Wadi Zaghra, South Sinai, Egypt. *Acta Geologica Sinica* (English Edition), 93(1): 50–73. DOI: 10.1111/1755-6724.13762

1 Introduction

Late Neoproterozoic rocks outcropping in southern Sinai form a part of the Nubian Shield, which was contiguous with the Arabian Shield before the Red Sea opening; together these two shields form the Arabian-Nubian Shield (ANS). The ANS represents the youngest juvenile continental crust on earth, which records events associated with the East African Orogeny (900–530 Ma; Stern, 1994). It was formed in Late Neoproterozoic time by prolonged accretion of oceanic island arc terranes due to late Neoproterozoic continental collision during closure of the Mozambique Ocean (e.g. Bentor, 1985; Stern, 1994; Meert, 2003; Stoesser and Frost, 2006; Johnson et al., 2013) that created many suture zones intruded by ophiolites (Abdelsalam and Stern, 1996; Stern, 1994; Stern et al., 2004; Ali et al., 2010; Khalil et al., 2014).

One of the most distinctive features of south Sinai is the many post-collisional calc-alkaline (ca. 635–590 Ma: Ediacaran) granitic suites and volcano-sedimentary successions (Bentor, 1985; Bentor and Eyal, 1987; Farahat

and Azer, 2011; Samuel et al., 2011; Be'eri-Shlevin et al., 2009, 2011; Abdelfadil et al., 2018). Older rocks, now comprising parts of the metamorphic complexes are subordinate, whereas ophiolitic rocks are completely lacking due to erosion associated with crustal uplift during the late collisional phase (Bentor, 1985; Stein, 2003; Jarrar et al., 2003; Eyal et al., 2013).

Within the Precambrian Basement Complex of Egypt four major volcano-sedimentary assemblages have been identified: (a) an oceanic ophiolitic assemblage; (b) an island arc volcano-sedimentary assemblage, (c) late orogenic Dokhan Volcanics-Hammamat Clastics assemblage; and (d) the within-plate Katharina volcanic-Elat conglomerates assemblage.

In Sinai, the first assemblage is absent. Several authors (El-Gaby, 1983; Ries et al., 1983; Stern et al., 1984; Furnes et al., 1985; Takla, 2002) have raised doubt about the presence of the second assemblage (the island arc) in Sinai, but others (e.g. Shimron, 1980; Bentor, 1985; Garfunkel, 1999; Mehanna et al., 2001; Eyal et al., 2010, 2013) have stressed its presence. The third assemblage (the volcano-sedimentary succession) is present in Sinai and is considered parallel to the Dokhan-Hammamat

* Corresponding author. E-mail: mokhles72@yahoo.com

succession in the Eastern Desert of Egypt [ED] (e.g. Schürmann, 1966; Bendor, 1985; El-Gaby et al., 1988, 2002; Samuel et al., 2001, 2011; Azer, 2007; El-Bialy, 2010; Be'eri-Shlevin et al., 2011; Abdelfadil et al., 2018). The within-plate Katharina volcanic assemblage is represented by alkaline/peralkaline rhyolitic flows, agglomerates and ignimbrites. They are unmetamorphosed and unfolded (Eyal and Hezkiyahu, 1980; Agron and Bendor, 1981; Bendor, 1985; Bendor and Eyal, 1987; Azer, 2006; Samuel et al., 2007; Azer et al., 2014). The Katharina Volcanics interfinger with the thick Elat Conglomerates in the Elat area (Bendor, 1985).

Four metamorphic complexes are distinguished in Sinai: Sa'al, Feiran-Solaf, Kid and Taba. The Sa'al metamorphic complex (SMC) represents the oldest (Be'eri-Shlevin et al., 2012; Eyal et al., 2013), and comprises three different formations: Ra'ayan (the oldest), Agramyia and Zaghra (the youngest).

Some authors have considered that the volcano-sedimentary succession around Wadi Zaghra belongs to an island arc assemblage (Shimron, 1980; Bendor, 1985; Shimron et al., 1993; Mehanna et al., 2001), but others considered that its volcanic had erupted in an ensialic continental arc setting (e.g. Furnes et al., 1985). El-Gaby et al. (2002) concluded that the whole Sa'al-Zaghra succession belongs to the ensialic Dokhan Volcanics and molasse-type epiclastic sediments (Hammamat Clastics).

Several studies on the Wadi Zaghra conglomerates revealed that they are either polymictic (e.g. Shimron et al., 1993; El-Gaby et al., 2002; Hegazi, 2006; Andresen et al., 2014) or oligomictic conglomerates (Mehanna et al., 2001) composed only of gneissic clasts. Most of the previous authors mentioned that the conglomerates were folded, metamorphosed under greenschist facies conditions, and subjected to deformation. Hassan et al. (2014) and Fowler et al. (2015) suggested that the whole Sa'al complex represents a low-grade metamorphosed and poly-deformed sequence, and that the earlier stage of metamorphism and deformation occurred during the breakup of Rodinia at a late Mesoproterozoic age. This assumption contradicts field observations and recent dating, as there is a time gap of ~400 Ma between the oldest two formations (Ra'ayan and Agramyia) and the Zaghra Formation (cf. Eyal et al., 2013; Andresen et al., 2014).

There is also contradiction among previous authors regarding the stratigraphic position of the Wadi Zaghra clastics relative to the surrounding intrusive rocks. They overlie gneisses and were intruded by synorogenic granodiorites, late orogenic biotite granites and post-orogenic leucogranites (Shimron et al., 1993; Mehanna et al., 2001). El-Gaby et al. (2002) reported that gneissose tonalite-granodiorites (not gneisses) are at the base of the Wadi Zaghra sequence and that quartz diorite-granodiorites separate the lower (older) Dokhan Volcanics and the upper (younger) Dokhan Volcanics. Andresen et al. (2014) concluded that the Wadi Zaghra metaconglomerates are completely surrounded by magmatic rocks emplaced after their deformation and metamorphism. These intrusive are diorite-granodiorite, monzogranite, and alkali-feldspar granite with zircon ages

of 614 ± 4 Ma, 605 ± 7 Ma and 622 ± 6 Ma, respectively (Andresen et al., 2014).

The proposed deposition age (635–615 Ma) of the Wadi Zaghra metasedimentary rocks by Andresen et al. (2014) is similar to that of the older unit of the nearby Rutig sedimentary succession (Samuel et al., 2011). Andresen et al. (2014) also mentioned that the Zaghra metasedimentary rocks are older than the whole Hammamat clastics. However, Samuel et al. (2011) and Be'eri-Shlevin et al. (2011) pointed out that the volcano-sedimentary succession at Wadi Rutig correlates with the Dokhan-Hammamat sequence.

The present paper deals with the geology and geochemistry of the volcano-sedimentary succession of Wadi Zaghra, with special emphasis on the metamorphic conditions that prevailed and the tectonic setting of the succession.

2 Regional Geological Background

The Wadi Zaghra volcano-sedimentary succession is exposed in the central part of southern Sinai, about 21 km NE of Saint Katharina Town (Fig. 1a). The study area covers about 58 km² and is characterized by rugged topography with moderate to high relief, and is traversed by Wadi Makhazein and Wadi Zaghra and its southern tributary Wadi Khadra.

Basement rocks in the mapped area include gneissose tonalite-granodiorite, the Zaghra volcano-sedimentary successions and calc-alkaline granites (Fig. 1b). The Zaghra successions unconformably overlie gneissose tonalite-granodiorite in the western part of the studied area. Based on field relationships, composition and metamorphism, the Zaghra succession can be divided into two units: (1) the lower Zaghra unit, which comprises lava flows and pyroclastics interbedded with metagraywackes, semi-metapelites and metapelites. The lava flows are represented by metabasaltic andesite, meta-andesite and metadacite. The pyroclastics are dominated by andesitic and dacitic metatuffs. The associated sediments are folded and deformed; and (2) the upper Zaghra unit, includes lava flows, pyroclastics and sedimentary layers. This unit differs from the lower one. Here the lava flows and pyroclastics are mainly of rhyolitic and dacitic composition. Basaltic andesites and andesites are lacking and the rocks are unmetamorphosed. The sediments also display different characteristics as compared to those of the lower Zaghra unit; they are formed mainly of litharenite to sublitharenite and minor arenite and are interbedded with thin (1–3 m), fine polymictic conglomerates. The pebbles of the conglomerates show progressive decrease in size upwards together with notable increase in roundness. The thin conglomerate beds are generally more mature than the thick metaconglomerates of the lower unit.

The upper Zaghra unit is separated from the lower unit by a thick layer (about 20 m) of polymictic conglomerate appearing on both sides of Wadi Zaghra. It is typically poorly sorted and contains rounded granitic, minor volcanic and rare pelite clasts of different sizes, up to 50 cm long (Fig. 2a). The clasts are highly deformed and

mostly stretched in an ENE–WSW direction (Fig. 2b). The granitoid clasts comprise essentially granodiorite. The volcanic clasts include andesite and dacite. The metapelitic clasts show sedimentary lamination with recrystallized chlorite, sericite and quartz. The silty/sandy matrix of the conglomerate clasts shows clear lamination and foliation, which also continue in these clasts without any offset indicating a post-depositional deformation event.

A small mass of quartz diorite-granodiorite intrudes into the metaconglomerates with a sharp contact in the western part of Wadi Zaghra against the metaconglomerate (Fig. 2c); its crystallization age is 614 ± 4 Ma, as reported by Andresen et al. (2014).

3 Petrography

3.1 The lower Zaghra unit

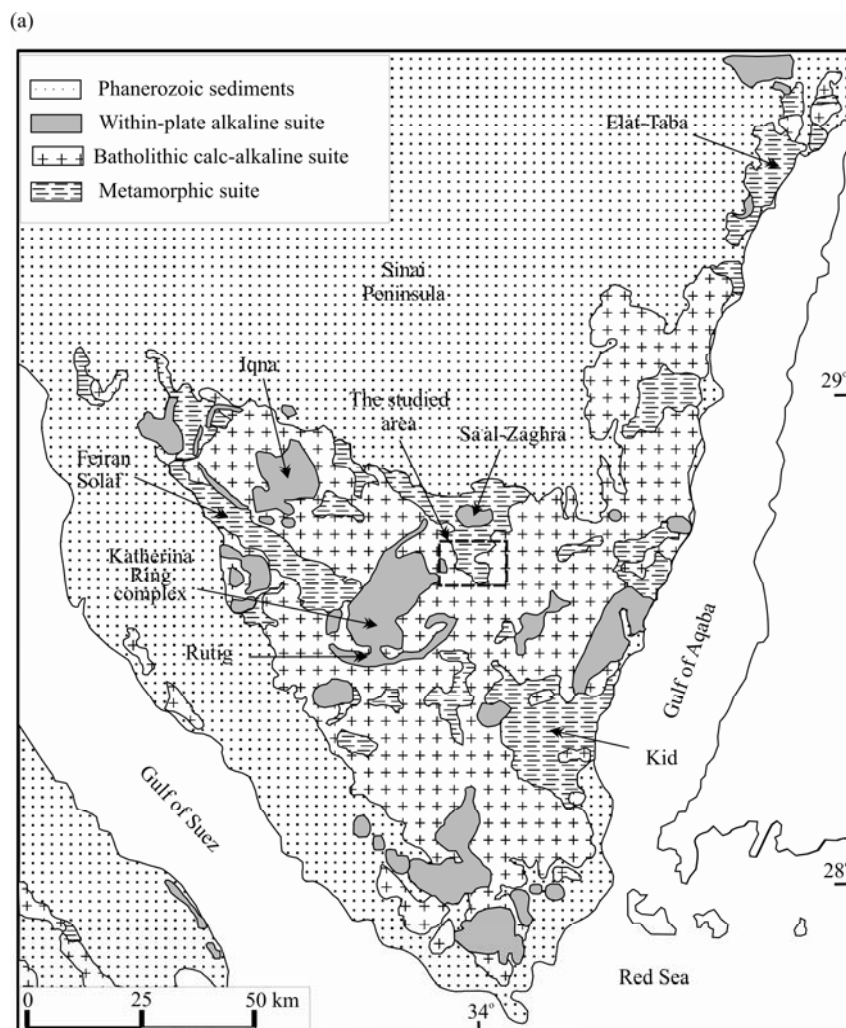
Volcanic rocks: The lava flows of the lower Zaghra unit are metamorphosed and represented by metabasaltic andesite, meta-andesite and metadacite. Metabasaltic andesites are of limited distribution and carry abundant plagioclase and augite phenocrysts set in a fine groundmass of plagioclase, augite, hornblende and chlorite with abundant opaque minerals. Porphyritic texture is common and fluidal texture is rarely observed. Tabular

plagioclase phenocrysts are zoned and altered to sericite. Augite forms subhedral stumpy crystals, commonly altered to chlorite and iron oxides along its margin.

The meta-andesites are commonly porphyritic and composed of abundant plagioclase and subordinate amounts of biotite, pyroxene, hornblende and secondary quartz. The plagioclase phenocrysts exhibit frequent albite-carlsbad twinning, and the crystals are saussuritized. Both biotite and amphibole occur as subhedral crystals and are extensively altered to iron oxides and chlorite. The accessory minerals present in the meta-andesite include opaque minerals, apatite and zircon.

The metadacite carry abundant plagioclase phenocrysts together with quartz and highly altered mafic minerals, set in a microcrystalline felsitic groundmass. Plagioclase phenocrysts are distinctly sericitized and show deformational features such as wavy extinction, slightly bent lamellae and kinked deformation. The dacites in contact with the diorite-granodiorite show a decussate texture where well-developed porphyritic hornblende crystals are frequently recrystallized into aggregates of secondary amphibole, biotite and/or chlorite (Fig. 3a).

Pyroclastics: The pyroclastics of the lower Zaghra unit are represented by lithic metatuffs and crystal metatuffs. The tuffs have a mineralogical composition similar to the



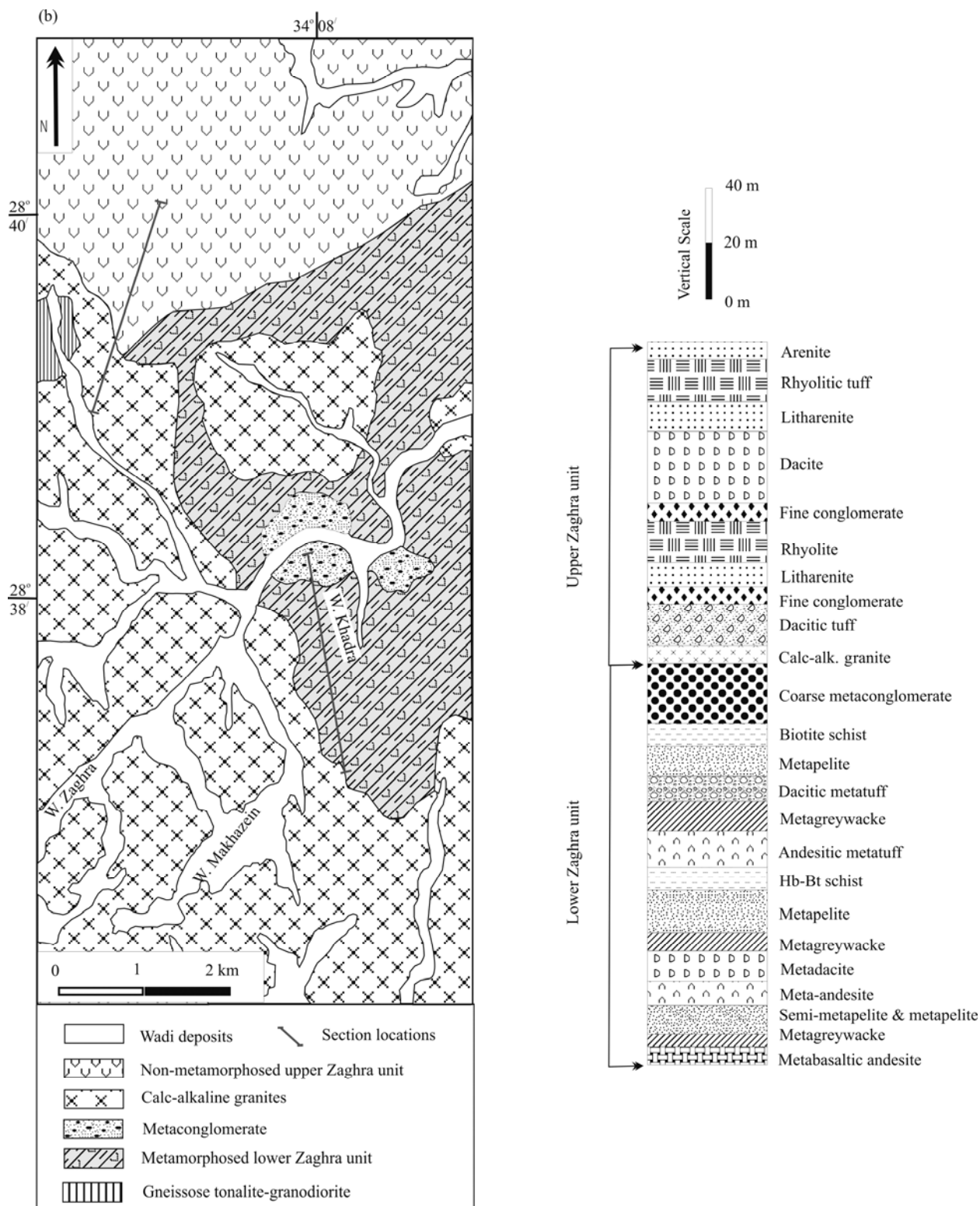


Fig. 1. (a) Geological map of Sinai (modified from Eyal et al., 1980) showing the locations of the metamorphic suites. The study area in Wadi Zaghra is marked; (b) Geological map of Zaghra area (modified from Mehanna et al., 2001) and measured columnar section of the volcano-sedimentary succession at Wadi Zaghra.

associated andesite-dacite rocks. The lithic metatuffs are banded and contain mainly lithic fragments of andesite, dacite and minor fragments of metamorphic rocks set in a microcrystalline groundmass with dust-size sericite and

opaques. The crystal metatuffs show sometimes a granoblastic polygonal (mosaic) texture characterized by polygonal crystals of nearly equal size with straight or curved grain boundaries. The metatuffs are flow banded

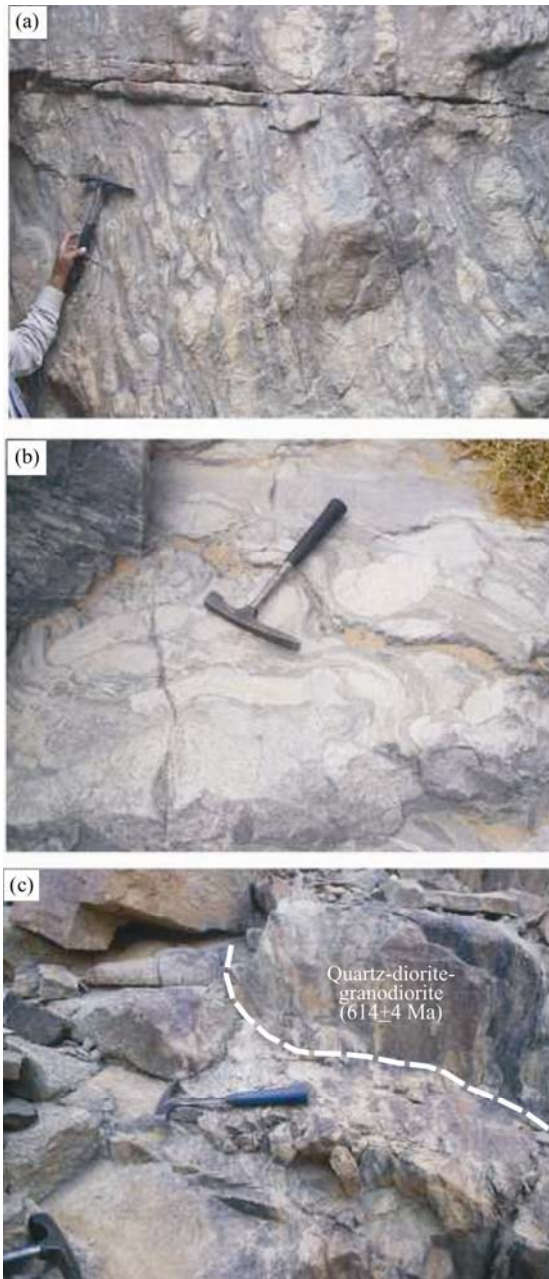


Fig. 2. (a) Zaghra metaconglomerates; (b) Close-up view of Zaghra polymictic metaconglomerates showing stretched clasts set in a foliated matrix; (c) Quartz diorite-granodiorite intrudes the metaconglomerates. Zircon ages are given by Andresen et al. (2014).

(Fig. 3b) and contain plagioclase, hornblende and quartz crystals. Their crystal fragments are minor hornblende, K-feldspars and opaques.

Interbedded sediments: The interbedded sedimentary layers in the lower Zaghra unit are differentiated into metagraywackes (both lithic and feldspathic), semi-metapelites, metapelites and schists. The lithic metagraywackes are fine- to medium-grained, poorly to moderately sorted sediments. They are composed of subangular quartz grains, subhedral grains of plagioclase

and microcline together with minor andesitic and dacitic rock fragments set in a matrix (>20 % by volume) composed of fine quartz, feldspar, chlorite, muscovite, biotite, epidote and opaque minerals. The feldspathic metagraywackes differ from the lithic metagraywackes in having more feldspar minerals and minor andesitic rock fragments. Both types of metagraywackes exhibit clear foliation and parallel alignment of elongate mineral grains (quartz, feldspars), biotite, amphibole and/or chlorite (Fig. 3c). In some samples, andalusite associated with muscovite is formed at the expense of K-feldspar (Fig. 3d).

The semi-metapelites are fine-grained and consist of quartz, feldspars, muscovite, biotite, and chlorite. Some semi-metapelites contain garnet either in the form of xenoblastic crystals having lobate form and containing inclusions (Fig. 3e), or as idiomorphic crystals free from inclusions. In some samples of the semi-metapelites, garnet porphyroblasts had grown over a foliated matrix indicating post-tectonic origin. The metapelites are composed of very fine-grained chlorite, quartz, plagioclase, fine opaques, epidote and biotite. In some samples lamination is still present. The schists are either biotite schist or hornblende biotite schist. The former schist is fine grained, gray to dark gray, and exhibits continuous schistosity sub-parallel to bedding. Biotite occurs as rather thin, elongate, flaky aggregates that show definite parallelism in a granoblastic matrix of quartz and saussuritized plagioclase. In some samples, the biotite flakes are disposed along two schistosity planes (Fig. 3f) with different orientation. Accessory minerals include opaques, apatite and zircon. The hornblende biotite schist is similar to biotite schist but contains less biotite flakes with the presence of green hornblende (Fig. 3g). Both types of schist contain chlorite developed at the expense of pre-existing biotite.

The metaconglomerates: The clasts of the metaconglomerates are represented by various granitoids with minor volcanics and rare metamorphic ones. The granitoid clasts are composed of anhedral, flattened quartz grains showing undulose extinction. Their feldspars are composed of either fine- to medium-sized crystals of K-feldspar or plagioclase. The K-feldspar occurs as anhedral microcline and lenticular perthite. The plagioclase occurs as subhedral crystals showing lamellar and pericline twinning and is commonly altered to sericite. The clasts contain variable amounts of muscovite and biotite flakes partially retrograded to chlorite. The dominant volcanic clasts are metadacites with a mineral assemblage of plagioclase + biotite + epidote + chlorite ± hornblende ± actinolite ± quartz and opaques. The composition, texture and metamorphic facies of these clasts are similar to the metadacites of the lower Zaghra unit. The metamorphic clasts are represented by semi-pelites characterized by fine-grained, ill-sorted quartz grains, feldspar, chlorite, epidote and opaques. In general, the clasts exhibit schistosity and parallel alignment of the mineral contents.

3.2 The upper Zaghra unit

Volcanic rocks: The lava flows of the upper unit at Zaghra are unmetamorphosed dacite, rhyodacite and

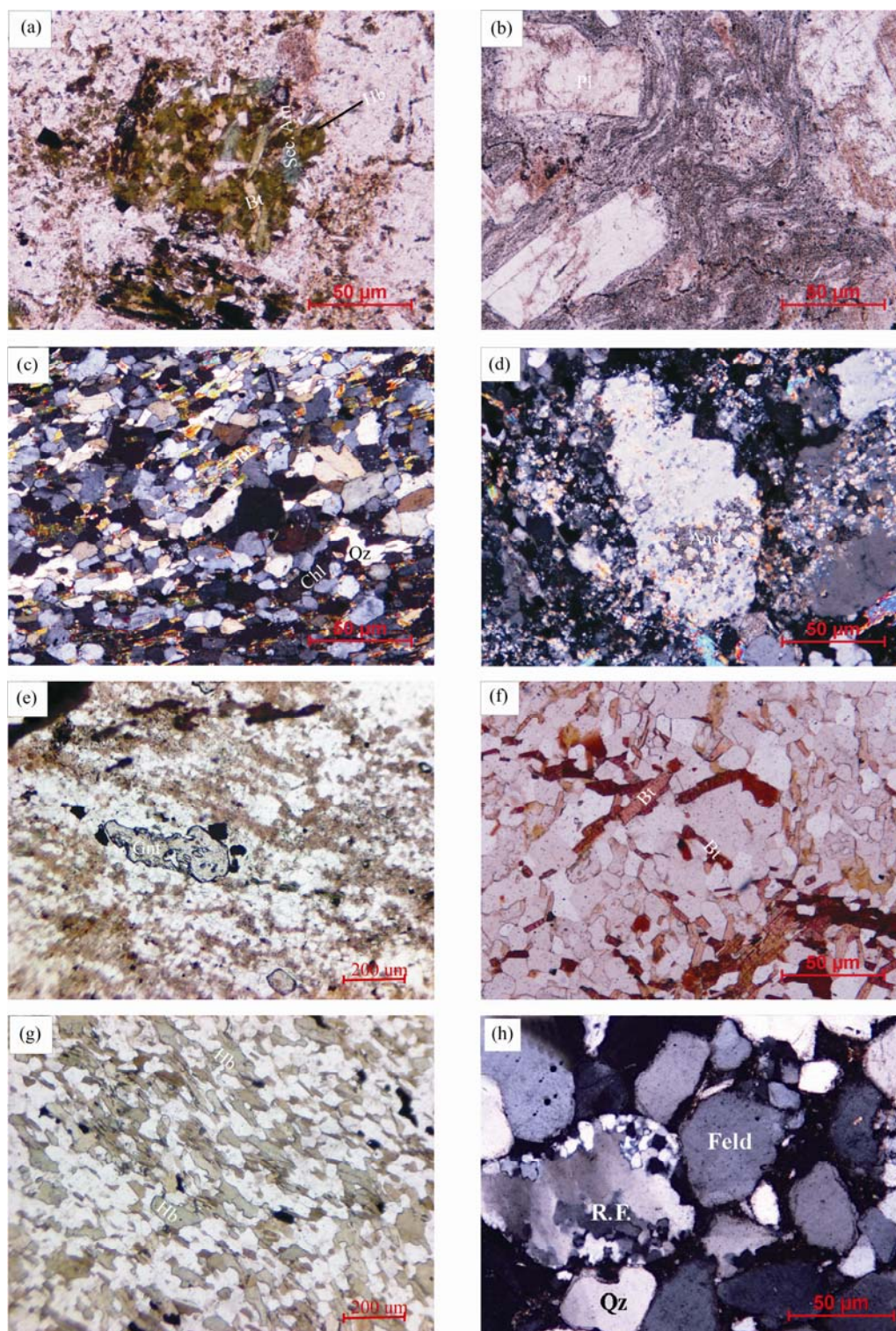


Fig. 3. (a) Biotite, secondary amphibole and chlorite flakes showing decussate texture pseudomorphous after primary amphibole in metamorphosed dacite. P.P.L.; (b) crystal metatuffs with flow banding. P.P.L.; (c) metagraywacke shows clear foliation and parallel alignment of elongate mineral constituents. C.N.; (d) andalusite associated with muscovite formed at the expense of K-feldspar in metagraywacke. C.N.; (e) xenoblastic garnet crystal with inclusions in semi-pelites. P.P.L.; (f) biotite flakes aligned along two schistosity planes in biotite schist. P.P.L.; (g) hornblende-biotite schist. P.P.L.; (h) rounded quartz and rock fragments in unmetamorphosed litharenite C.N..

Mineral abbreviations Sec Amp: secondary amphibole; Pl: plagioclase; Chl: Chlorite; Qz: quartz; And: Andalusite; Gnt: Garnet; Bt: biotite; Hb: hornblende; R.F: rock fragment; Feld: feldspar.

rhyolite. The dacites are composed of abundant plagioclase phenocrysts, infrequent hornblende and biotite and rare alkali-feldspars and quartz, in a microcrystalline groundmass. Most of the plagioclase crystals are albite and oligoclase. The hornblende occurs as anhedral crystals and the biotite is present as subhedral crystals or as fine flakes in the groundmass. The main accessory minerals are opaques, apatite and zircon.

The rhyodacites are similar to the dacites but contain more phenocrysts of sanidine and quartz. The plagioclases are mostly of albite and oligoclase composition. The quartz phenocrysts occur as bipyramidal deeply embayed crystals. Biotite is present in the form of fine flakes. Opaque minerals are infrequent.

The rhyolites consist of phenocrysts of quartz and alkali feldspars with minor plagioclase and biotite in a microcrystalline groundmass.

All these volcanics exhibit a typical porphyritic texture and the groundmass exhibits myrmekitic, micrographic and/or spherulitic texture.

Pyroclastics: The pyroclastics of the upper Zaghra unit differ from those encountered in the lower unit in the presence of quartz and K-feldspars in subordinate amounts, and in having a more rhyolitic composition. Lithic tuffs are poorly sorted and consist mainly of dacite and rhyolite with minor granite lithic fragments embedded in a cryptocrystalline groundmass. The crystal fragments present comprise angular quartz and feldspars. Crystal tuffs are abundant and are composed mainly of crystal fragments embedded in a tuffaceous groundmass.

Interbedded sediments: The sedimentary beds intercalated with the volcanics and pyroclastics of the upper Zaghra unit are represented mainly by litharenites (Fig. 3h), sublitharenites and minor arenites. The first contain abundant quartz, chert and quartzite with feldspars embedded in an argillaceous matrix (< 10%). Their rock fragments exceed the feldspars. The second have less rock fragments than the litharenite. The arenites are formed of well-sorted, subrounded to rounded quartz grains and contain less than 10% argillaceous matrix.

4 Analytical Methods

Electron microprobe analyses of mineral phases in the studied rocks were acquired using a five-spectrometer JEOL JXA-8200 electron microprobe at the Geological and Planetary Sciences (GPS) Division Analytical Facility, California Institute of Technology, Pasadena, California, USA. Operating conditions were 15 kV accelerating voltage, 25 nA beam current, a focused beam (1 µm), 20 s on-peak and 10 s off-peak counting times. A mix of natural (Amelia albite, Asbestos microcline) and synthetic (forsterite, fayalite, Mn-olivine, anorthite, NiO, TiO₂, Cr₂O₃) mineral standards were used, and the CITZAF matrix correction procedure.

The chemical compositions of the metavolcanics of the lower unit of Zaghra succession and that of the volcanics of the upper unit of the succession, in addition to those of the metasedimentary rocks encountered in the lower unit were determined by a combination of X-ray fluorescence (XRF) and ICP-mass spectrometry, at the Institute of

Mineralogy, Clausthal Technical University, Germany and at ACME Analytical Laboratories Limited, Vancouver, Canada. The results of the analyses of the major, trace and rare earth elements of the volcanic rocks are given in Tables 1 and 2.

5 Discussions

5.1 Mineral chemistry

The analyses were carried out on plagioclase feldspar, pyroxene, primary and secondary amphibole crystals from

Table 1 Major oxides (wt%) and trace elements (ppm) of the studied lower volcanic unit

Rock type	BTA	A	D	TD	TD	TD	D
Sample No.	16	2A	4	18	24	24A	Kh10
SiO ₂	54.66	57.93	67.31	64.34	66.82	65.31	68.10
TiO ₂	1.29	1.08	0.54	0.78	0.56	0.75	0.50
Al ₂ O ₃	17.15	16.75	14.96	15.76	15.89	16.05	13.64
Fe ₂ O ₃	7.98	6.79	4.24	4.50	2.95	3.53	4.19
MnO	0.18	0.12	0.08	0.07	0.05	0.07	0.11
MgO	4.06	3.89	1.74	2.03	1.14	1.31	4.10
CaO	5.85	5.51	3.8	3.64	2.54	2.81	1.40
Na ₂ O	4.40	3.75	4.03	4.26	4.02	3.75	3.58
K ₂ O	1.80	1.90	2.23	3.16	4.36	4.03	1.65
P ₂ O ₅	0.32	0.27	0.12	0.23	0.11	0.13	0.17
L.O.I.	1.76	1.33	0.52	0.86	0.83	1.65	-
Total	99.45	99.32	99.57	99.63	99.27	99.39	97.44
NK/A	0.52	0.49	0.61	0.69	0.79	0.72	0.56
Suite Index	3.3	2.1	1.6	2.6	2.9	2.7	1.1
Ba	437	613	662	799	780	774	366
Co	23	20	12.1	18	-	-	10
Cr	74	125	68	47	12	14	9
Cu	27	39	61.2	32	12	15	56
Ga	22	20.6	17.8	19	18.8	18.4	-
Nb	8	8	12	9	8	7	7
Ni	47	66	44.3	24	2	3	15
Pb	26	13	19.6	18	22	21	111
Rb	36	43	32.3	60	107	96	48
Sr	687	980	367.9	583	388	409	1525
V	174	138	70.6	51	59	74	72
Y	15	13	22.3	17	18	17	19
Zn	154	112	72.9	88	52	54	124
Zr	183	155	222.1	263	221	219	259
Sc	15.5	11.2	8.9	10.1	9	7	-
Th	4.2	4.8	11	7	9.2	9.9	14
Hf	4.7	4.1	7	6.4	7.6	6.4	-
Ta	0.4	0.4	0.6	0.7	0.7	0.6	-
U	1.7	1.2	3.2	3	4.4	4.5	-
Cs	9.5	4.2	-	3.7	-	-	-
La	18.9	24.3	-	27.5	29.69	26.81	23.7
Ce	41.2	51.5	-	55.5	60.01	55.22	62.5
Pr	5.66	6.64	-	7.01	6.59	5.88	5.78
Nd	22.3	27.3	-	27.7	24.17	20.72	22
Sm	4.89	5.71	-	5.5	4.63	3.69	4.31
Eu	1.48	1.6	-	1.42	1.14	0.96	0.99
Gd	3.59	4.96	-	4.13	3.38	2.93	2.86
Tb	0.56	0.72	-	0.68	0.57	0.43	0.45
Dy	3.05	4.08	-	4.01	3.13	2.53	2.88
Ho	0.58	0.79	-	0.83	0.61	0.53	0.59
Er	1.56	2.05	-	2.26	1.66	1.43	1.69
Tm	0.23	0.29	-	0.33	0.27	0.25	0.26
Yb	1.51	1.84	-	2.14	1.97	1.64	1.63
Lu	0.23	0.27	-	0.34	0.31	0.28	0.25
ΣREE	105.74	132.05	-	139.35	138.13	123.3	129.89
Eu/Eu*	1.08	0.92	-	0.91	0.88	0.89	0.86
(La/Yb) _N	8.98	9.47	-	9.22	10.81	11.73	10.43
(La/Sm) _N	2.50	2.75	-	3.23	4.14	4.69	3.55
(Gd/Yb) _N	1.97	2.23	-	1.60	1.42	1.48	1.45
(Ce/Yb) _N	7.58	7.77	-	7.20	8.46	9.35	10.65

* Rock name according to TAS classification

Suite Index $\sigma = (\text{Na}_2\text{O} + \text{K}_2\text{O})^2 / \text{SiO}_2 - 43$ (Rittmann, 1962)

Table 2 Major oxides (wt%) and trace elements (ppm) of the upper volcanic unit

Rock type	TD	TD	TD	TD	R	R	R	R	R	R
Sample No.	3	5	11	30	32	33	34	39	40	41
SiO ₂	65.75	66.54	67.58	68.32	72.32	72.94	73.09	72.54	74.23	73.68
TiO ₂	0.72	0.69	0.59	0.55	0.34	0.17	0.32	0.23	0.16	0.26
Al ₂ O ₃	16.26	15.98	15.77	15.63	14.36	14.29	13.91	14.22	13.11	13.03
Fe ₂ O ₃	3.12	3.45	3.13	2.71	1.72	0.88	1.49	1.73	1.76	2.37
MnO	0.09	0.09	0.10	0.08	0.06	0.04	0.03	0.04	0.02	0.05
MgO	0.99	0.77	0.61	0.68	0.37	1.02	0.53	0.25	0.20	0.75
CaO	2.53	2.35	2.15	2.12	0.81	0.22	1.13	0.53	0.28	0.92
Na ₂ O	4.91	5.34	4.74	4.74	5.23	4.05	3.96	5.85	4.22	4.49
K ₂ O	3.64	3.15	3.45	3.60	4.08	4.45	4.68	3.07	4.50	3.25
P ₂ O ₅	0.17	0.16	0.15	0.14	0.08	0.04	0.05	0.04	0.03	0.08
L.O.I.	0.85	1.00	0.99	0.80	0.56	0.55	0.56	0.55	0.54	0.60
Total	99.03	99.52	99.26	99.37	99.93	98.65	99.75	99.05	99.05	99.48
NK/A	0.77	0.78	0.76	0.79	0.96	0.89	0.93	0.92	0.99	0.87
Suite Index	3.2	3.1	2.7	2.7	3.0	2.4	2.5	1.6	2.4	2.0
Ba	891	739	852	880	790	747	742	641	408	714.5
Co	17	15	11	11	9	4	-	6	6	8.5
Cr	24	16	14	19	10	0	9	6	15	2.3
Cu	38	27	37	23	3	83	8	20	12	86.6
Ga	20	20.5	19.6	19.3	18.2	-	13.9	20.3	20	18.2
Nb	10	11	10	12	15	11	10	13	14	13
Ni	7	8	8	11	7	5	1	5	8	22.4
Pb	20	27	44	16	22	32	23	349	155	49.2
Rb	77	67	89	65	109	134	156	88	119	66.1
Sr	430	338	362	190	184	242	185	112	57	199.1
V	37	36	34	36	8	0	51	5	3	20.6
Y	27	30	29	26	30	27	26	38	46	27.7
Zn	90	81	102	28	63	50	31	55	48	65.1
Zr	337	331	301	325	316	152	231	338	341	278.3
Sc	9.4	10.6	9	8.5	6.7	-	3	5.1	5.1	6.1
Th	7.7	7.3	7.6	7.3	9.1	17	14.2	11.4	12.2	13.1
Hf	8.2	8.2	7.5	7.5	7.7	-	7.8	9.4	10.1	9.9
Ta	0.6	0.7	0.6	0.7	0.8	-	0.8	0.9	0.9	0.7
U	1.7	3.4	2	2.6	3.8	-	6.1	3.4	3.2	4.1
Cs	3.9	2.6	3.9	2.4	1.5	-	-	0.7	1.3	-
La	31.9	34.3	31.9	33.1	37.8	-	44.74	39.3	41.4	-
Ce	65.4	69.4	65.2	67.8	78.1	-	81.97	80.4	85.1	-
Pr	8.12	8.53	7.94	8.31	9.5	-	9.58	9.69	10.49	-
Nd	31.6	33.3	30.7	31.6	36	-	34.02	36.5	39.4	-
Sm	6.48	6.84	6.28	6.62	7.3	-	6.65	7.42	8.24	-
Eu	1.67	1.81	1.67	1.68	1.2	-	1.31	0.73	0.41	-
Gd	5.51	5.84	5.32	5.61	5.9	-	6.42	6.26	7.14	-
Tb	0.89	0.94	0.86	0.9	1	-	0.97	1.08	1.27	-
Dy	5.25	5.59	5.14	5.38	5.9	-	5.28	6.62	7.96	-
Ho	1.06	1.14	1.05	1.08	1.2	-	1.11	1.38	1.67	-
Er	2.93	3.07	2.86	2.97	3.3	-	2.96	3.87	4.71	-
Tm	0.44	0.46	0.44	0.44	0.5	-	0.48	0.58	0.72	-
Yb	2.84	2.96	2.8	2.85	3.3	-	3.04	3.76	4.65	-
Lu	0.44	0.47	0.44	0.45	0.50	-	0.49	0.6	0.73	-
∑REE	164.53	174.65	162.60	168.79	191.50	-	199.02	198.19	213.89	-
Eu/Eu*	0.85	0.88	0.88	0.84	0.56	-	0.61	0.33	0.16	-
(La/Yb) _N	8.06	8.31	8.17	8.33	8.22	-	10.56	7.50	6.39	-
(La/Sm) _N	3.18	3.24	3.28	3.23	3.34	-	4.34	3.42	3.24	-
(Gd/Yb) _N	1.60	1.63	1.57	1.63	1.48	-	1.75	1.38	1.27	-
(Ce/Yb) _N	6.40	6.51	6.47	6.61	6.57	-	7.49	5.94	5.08	-

* Rock name according to TAS classification. Suite Index $\sigma = (\text{Na}_2\text{O} + \text{K}_2\text{O})/\text{SiO}_2 - 43$ (Rittmann, 1962)

the metabasaltic andesite, and on plagioclase and alkali feldspars, and biotite crystals from the metadacite of the lower Zaghra unit. Analyses were also carried out on plagioclase and alkali feldspars, amphibole, and biotite crystals from dacite, and on plagioclase and alkali feldspar crystals from the rhyolites of the upper unit of Zaghra succession. All analyses were on single selected spots. The structural formulae of the analyzed minerals were calculated using Minpet software (Richard, 1995).

Feldspars: The chemical composition of the analyzed feldspars is given in Tables 3–8 and in Fig. 4a. The

plagioclase of the metabasaltic andesite has an average composition of Ab₄₈ An₅₀ Or₂, i.e. andesine-labradorite, whereas the plagioclase from the metadacite has an average composition of Ab₇₅ An₂₄ Or₁, i.e. oligoclase. The co-existing alkali feldspar with the latter plagioclase has an average composition of Ab₁₃ An₁ Or₈₆, i.e. sanidine. The feldspars from the dacite of the upper unit of the Zaghra succession have the following average composition: plagioclase, Ab₈₄ An₁₄ Or₂ (oligoclase), and the alkali feldspar, Ab₄₉ An₆ Or₄₅ (sanidine). This means that the plagioclase from the dacite has more sodium and

Table 3 Representative microprobe analyses (wt%) of plagioclase feldspars for metabasaltic andesite, Zaghra lower unit

Points	1	2	3	4	5	6	7	8	9
SiO ₂	51.55	51.74	52.36	54.93	57.81	55.29	53.35	53.36	62.56
TiO ₂	0.10	0.10	0.10	0.10	0.08	0.11	0.10	0.10	0.06
Al ₂ O ₃	28.98	28.89	28.34	27.12	25.07	26.58	27.78	27.82	22.24
FeO	0.68	0.71	0.68	0.63	0.46	0.67	0.77	0.75	0.35
MnO	0.00	0.00	0.00	0.00	0.01	0.00	0.00	0.00	0.00
MgO	0.15	0.14	0.10	0.08	0.05	0.08	0.15	0.10	0.02
CaO	12.35	12.43	11.99	11.21	7.76	9.81	10.73	11.34	3.96
Na ₂ O	4.10	4.03	4.54	5.52	6.74	5.68	4.92	4.90	8.42
K ₂ O	0.35	0.37	0.19	0.24	0.47	0.31	0.44	0.24	1.27
Total	98.26	98.41	98.30	99.83	98.45	98.53	98.24	98.61	98.88
Number of cations on the basis of 32 oxygens									
Si	9.550	9.571	9.681	9.980	10.529	10.131	9.846	9.820	11.243
Ti	0.014	0.014	0.014	0.014	0.011	0.014	0.014	0.013	0.008
Al	6.323	6.293	6.170	5.803	5.378	5.736	6.038	6.030	4.707
Fe ²⁺	0.105	0.110	0.105	0.095	0.070	0.103	0.118	0.115	0.053
Mn	0.000	0.000	0.000	0.000	0.001	0.000	0.001	0.000	0.000
Mg	0.043	0.038	0.028	0.021	0.014	0.022	0.041	0.028	0.004
Ca	2.452	2.464	2.376	2.183	1.514	1.926	2.121	2.235	0.762
Na	1.474	1.446	1.628	1.946	2.382	2.018	1.761	1.748	2.934
K	0.083	0.088	0.045	0.057	0.109	0.071	0.105	0.057	0.290
Total	20.044	20.024	20.047	20.099	20.008	20.021	20.045	20.046	20.001
Ab	36.8	36.2	40.2	46.5	59.5	50.3	44.2	43.3	73.6
An	61.2	61.6	58.7	52.2	37.8	48.0	53.2	55.3	19.1
Or	2.1	2.2	1.1	1.4	2.7	1.8	2.6	1.4	7.3

less calcium than that of the metadacite, and that the alkali feldspar of the dacite has more sodium and less potassium than that of the metadacite. The plagioclase feldspars from the rhyolite have an average composition of Ab₉₈ An₁ Or₁ (i.e. albite), whereas the alkali feldspars have an average composition of Ab₄ An_{0.1} Or₉₆ (i.e. orthoclase).

Amphiboles: The amphiboles are present only in the metabasaltic andesite and in the dacites; no amphibole crystals have been identified in the metadacites. The microprobe analyses given in Table 9 and Fig. 4b show that the amphiboles of the metabasaltic andesites are calcic in composition and can be classified as actinolitic hornblende and magnesio-hornblende, according to the classification of Leake (1978). Most amphiboles are of secondary origin. Primary amphibole crystals found in the dacites of the upper Zaghra unit can be classified as edenitic hornblende.

Clinopyroxenes: The clinopyroxenes are present only as tiny inclusions within the amphiboles of metabasaltic andesite. The microprobe analyses of these pyroxenes (Table 9) show that there is a limited variation in their composition. On average, the composition of the pyroxene is Wo₃₉ En₄₁ Fs₂₀, i.e., augite, according to the classification of Morimoto (1988).

Biotites: Biotites are encountered both in the metadacites and in the dacites. Their chemical composition is given in Tables 10–11. Figure 4c shows that the plot of the composition of these biotites using the triangular diagram of Nachit et al. (2005). The diagram shows that the biotites from the metadacites are mainly re-equilibrated primary biotites, whereas the biotites from the dacites are primary biotites.

5.2 Whole-rock geochemistry

Volcanic rocks: Figure 5a is the TAS diagram

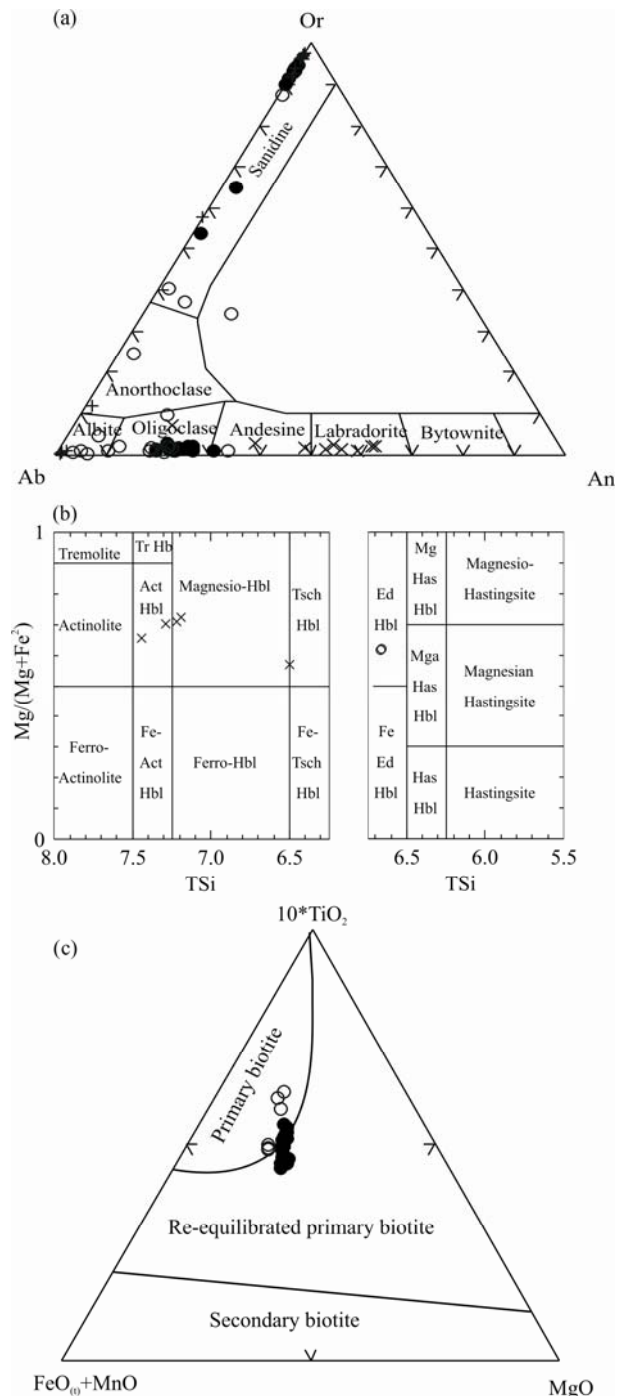


Fig. 4. (a), Or-Ab-An ternary diagram of the analyzed feldspars (after Deer et al., 1992); x = lower andesite; • = lower dacite; o = upper dacite; + = upper rhyolite; (b), Classification of the analyzed amphiboles (after Leake, 1997); (c) TiO₂-FeO₀+MnO-MgO ternary diagram of the analyzed biotites (after Nachit et al., 2005). x = lower andesite; • = lower dacite; o = upper dacite.

recommended for the classification of volcanic rocks (Le Maitre, 2002). The diagram shows that the volcanic rocks of the Zaghra lower unit vary from basaltic trachyandesite to andesite and dacite (two samples are trachydacite). On the other hand, the volcanic rocks of the Zaghra upper unit

Table 4 Representative microprobe analyses (wt%) of plagioclase feldspars for metadacite, Zaghra lower unit

Points	10	11	12	13	14	15	16	17	18	19	20
SiO ₂	61.51	61.53	61.02	60.09	60.48	61.36	61.02	58.98	60.45	61.20	62.87
TiO ₂	0.01	0.02	0.00	0.01	0.00	0.00	0.02	0.02	0.03	0.05	0.00
Al ₂ O ₃	23.34	23.00	23.49	23.54	22.99	23.28	23.74	24.32	24.34	23.32	23.44
FeO	0.92	0.36	0.23	0.29	0.26	0.18	0.31	0.37	0.31	0.55	0.13
MnO	0.00	0.00	0.00	0.00	0.00	0.00	0.01	0.01	0.01	0.02	0.00
MgO	0.01	0.00	0.00	0.00	0.00	0.00	0.00	0.00	0.00	0.00	0.00
CaO	4.90	4.78	5.12	5.50	4.37	4.84	5.42	6.54	5.60	5.02	4.91
Na ₂ O	8.93	9.08	8.87	8.66	8.96	8.92	8.57	8.09	8.45	8.87	9.03
K ₂ O	0.20	0.25	0.25	0.23	0.48	0.21	0.24	0.19	0.24	0.24	0.20
Total	99.82	99.02	98.98	98.32	97.54	98.79	99.33	98.52	99.43	99.27	100.58
Number of cations on the basis of 32 oxygens											
Si	10.988	11.052	10.969	10.894	11.027	11.030	10.934	10.706	10.831	10.983	11.088
Ti	0.001	0.003	0.000	0.002	0.000	0.000	0.002	0.003	0.004	0.006	0.000
Al	4.911	4.865	4.974	5.025	4.936	4.929	5.010	5.200	5.136	4.929	4.869
Fe ²⁺	0.137	0.054	0.035	0.043	0.040	0.027	0.047	0.056	0.047	0.083	0.019
Mn	0.000	0.000	0.000	0.000	0.000	0.000	0.001	0.001	0.001	0.003	0.000
Mg	0.002	0.000	0.000	0.000	0.000	0.000	0.000	0.000	0.000	0.000	0.000
Ca	0.938	0.921	0.986	1.069	0.853	0.933	1.041	1.272	1.075	0.965	0.927
Na	3.095	3.163	3.091	3.045	3.169	3.111	2.976	2.848	2.935	3.087	3.089
K	0.045	0.058	0.057	0.054	0.112	0.047	0.056	0.045	0.056	0.054	0.045
Total	20.117	20.116	20.112	20.132	20.137	20.077	20.067	20.131	20.085	20.110	20.037
Ab	75.9	76.4	74.8	73.1	76.7	76.0	73.1	68.4	72.2	75.2	76.1
An	23.0	22.2	23.9	25.6	20.6	22.8	25.5	30.5	26.4	23.5	22.8
Or	1.1	1.4	1.4	1.3	2.7	1.1	1.4	1.1	1.4	1.3	1.1
Points	21	22	23	24	25	26	27	28	29	30	
SiO ₂	62.65	62.34	61.88	61.68	63.56	63.00	62.70	62.18	62.71	62.29	
TiO ₂	0.00	0.00	0.00	0.02	0.01	0.00	0.01	0.01	0.00	0.01	
Al ₂ O ₃	23.44	23.73	24.02	23.94	22.87	23.41	23.44	24.15	23.73	23.96	
FeO	0.20	0.19	0.17	0.34	0.50	0.15	0.14	0.22	0.18	0.32	
MnO	0.00	0.01	0.01	0.00	0.00	0.02	0.00	0.00	0.00	0.01	
MgO	0.00	0.00	0.00	0.00	0.00	0.00	0.00	0.00	0.00	0.00	
CaO	4.97	5.35	5.55	5.54	4.13	4.54	4.68	5.57	5.19	5.28	
Na ₂ O	8.82	8.63	8.45	8.54	9.58	8.97	9.00	8.50	8.79	8.70	
K ₂ O	0.31	0.34	0.37	0.23	0.23	0.26	0.23	0.16	0.22	0.21	
Total	100.39	100.59	100.45	100.29	100.88	100.35	100.20	100.79	100.82	100.78	
Number of cations on the basis of 32 oxygens											
Si	11.075	11.014	10.955	10.943	11.184	11.120	11.093	10.957	11.041	10.985	
Ti	0.001	0.000	0.000	0.002	0.001	0.000	0.001	0.002	0.000	0.001	
Al	4.881	4.937	5.007	5.003	4.739	4.867	4.884	5.012	4.921	4.976	
Fe ²⁺	0.030	0.027	0.026	0.050	0.073	0.023	0.021	0.033	0.026	0.047	
Mn	0.000	0.002	0.001	0.001	0.000	0.003	0.000	0.000	0.000	0.001	
Mg	0.000	0.000	0.000	0.000	0.000	0.000	0.000	0.000	0.000	0.000	
Ca	0.942	1.012	1.053	1.053	0.778	0.859	0.888	1.053	0.978	0.997	
Na	3.024	2.958	2.900	2.937	3.270	3.072	3.089	2.906	3.001	2.976	
K	0.071	0.077	0.083	0.051	0.053	0.059	0.051	0.037	0.050	0.047	
Total	20.024	20.027	20.025	20.040	20.098	20.003	20.027	20.000	20.017	20.030	
Ab	74.9	73.1	71.9	72.7	79.7	77.0	76.7	72.7	74.5	74.0	
An	23.3	25.0	26.1	26.1	19.0	21.5	22.0	26.4	24.3	24.8	
Or	1.8	1.9	2.1	1.3	1.3	1.5	1.3	0.9	1.2	1.2	

are trachydacites and rhyolite. Figure 5b is a plot of K₂O against SiO₂ (Ewart, 1982) and indicates that the volcanics of the Zaghra lower unit vary from medium-K to high-K rocks (especially the dacites), whereas the volcanics of the Zaghra upper unit are mainly high-K rocks. All the volcanics belong to the calc-alkaline series, according to the AFM diagram of Irvine and Baragar (1971; Fig. 5c). Furthermore, the calculated Suite Index σ of Rittmann (1962) is <4, which is characteristic of the calc-alkaline series, the index varying among the samples from 1.1 (strong calcalkaline) to 3.3 (weak calcalkaline), but mostly lies between 1.8 and 3.0 (average calcalkaline). The studied suite depicts smooth variation where TiO₂, FeO_t, CaO and P₂O₅ progressively decrease with gradual increase in SiO₂. Al₂O₃ of the lower volcanics decreases with silica increase up to ~65wt% and then increases with increasing silica followed by a marked decrease at

~68wt% SiO₂ (Fig. 6).

The trace element data show that Zr and Y increase from the basaltic andesite to andesite and dacite of the lower unit, accompanied by a decrease in Sr. Moreover, Rb and Ba increase up to ~68wt% SiO₂ and then decrease. The contents of Rb and Y increase from dacite to rhyolite of the upper unit, accompanied by a decrease in Sr (Fig. 6). The N-type MORB normalized multi-element diagram for the basaltic andesites and andesites show strong enrichment of large ion lithophile elements (LILE) compared to the high field strength elements (HFSE). They exhibit Ta-Nb anomalies (Fig. 7a). Dacites of the lower unit are generally more enriched in both LILE and HFSE with negative anomalies in P and Ti. The MORB normalized multi-element diagram of silicic rocks of the upper unit (dacites and rhyolites) display strong enrichment of LILE relative to the HFSE with negative Ta

Table 5 Representative microprobe analyses (wt%) of alkali feldspars for metadacite, Zaghra lower unit

Points	31	32	33	34	35	36	37	38	39	40
SiO ₂	63.39	63.74	73.18	64.72	64.92	65.33	65.32	65.23	65.30	64.85
TiO ₂	0.04	0.04	0.00	0.04	0.04	0.03	0.03	0.01	0.03	0.06
Al ₂ O ₃	18.21	18.35	15.34	18.56	18.43	19.31	18.41	18.43	18.57	18.44
FeO	0.51	0.38	0.16	0.11	0.10	0.08	0.08	0.12	0.12	0.15
MnO	0.00	0.01	0.00	0.00	0.00	0.02	0.03	0.00	0.00	0.00
MgO	0.00	0.00	0.00	0.00	0.00	0.00	0.00	0.00	0.00	0.00
CaO	0.05	0.05	0.29	0.02	0.03	0.61	0.01	0.02	0.01	0.04
Na ₂ O	0.71	0.74	3.95	0.65	0.57	3.66	0.73	0.72	0.92	1.07
K ₂ O	15.55	15.50	7.25	15.62	15.92	11.28	15.62	15.66	15.39	15.07
Total	98.46	98.81	100.17	99.72	100.01	100.32	100.23	100.19	100.34	99.68
Number of cations on the basis of 32 oxygens										
Si	11.923	11.930	12.839	11.971	11.986	11.856	12.012	12.006	11.988	11.981
Ti	0.005	0.005	0.000	0.005	0.006	0.004	0.004	0.001	0.004	0.008
Al	4.035	4.044	3.169	4.042	4.007	4.127	3.986	3.994	4.015	4.011
Fe ²⁺	0.080	0.059	0.024	0.016	0.015	0.012	0.012	0.018	0.019	0.024
Mn	0.000	0.002	0.000	0.000	0.000	0.002	0.005	0.000	0.000	0.000
Mg	0.000	0.000	0.000	0.000	0.000	0.000	0.000	0.000	0.000	0.000
Ca	0.010	0.010	0.054	0.004	0.006	0.119	0.002	0.005	0.002	0.007
Na	0.259	0.269	1.345	0.233	0.205	1.287	0.260	0.257	0.329	0.384
K	3.731	3.702	1.624	3.685	3.750	2.611	3.665	3.677	3.606	3.553
Total	20.043	20.021	19.055	19.956	19.975	20.018	19.946	19.958	19.963	19.968
Ab	6.5	6.8	44.5	5.9	5.2	32.0	6.6	6.5	8.4	9.7
An	0.3	0.3	1.8	0.1	0.2	3.0	0.1	0.1	0.1	0.2
Or	93.3	93.0	53.7	94.0	94.7	65.0	93.3	93.3	91.6	90.1

Table 6 Representative microprobe analyses (wt%) of alkali feldspars for dacite, Zaghra upper unit

Points	55	56	57	58	59
SiO ₂	64.15	63.9	67.45	61.73	64.78
TiO ₂	0.02	0.00	0.00	0.03	0.01
Al ₂ O ₃	18.25	19.13	18.36	21.56	19.59
FeO	0.05	0.12	0.04	0.16	0.20
MnO	0.00	0.00	0.00	0.00	0.00
MgO	0.00	0.00	0.00	0.00	0.02
CaO	0.15	0.42	0.63	3.55	1.46
Na ₂ O	1.34	7.02	7.90	5.42	6.53
K ₂ O	14.91	7.52	4.06	5.90	6.58
Total	98.87	98.11	98.44	98.35	99.17
Number of cations on the basis of 32 oxygens					
Si	11.962	11.766	12.103	11.315	11.745
Ti	0.003	0.000	0.000	0.004	0.002
Al	4.008	4.148	3.881	4.653	4.182
Fe ²⁺	0.007	0.019	0.006	0.025	0.031
Mn	0.000	0.000	0.000	0.000	0.000
Mg	0.000	0.000	0.000	0.000	0.005
Ca	0.029	0.083	0.121	0.698	0.284
Na	0.485	2.507	2.747	1.926	2.295
K	3.547	1.766	0.930	1.379	1.522
Total	20.041	20.289	19.788	20.000	20.066
Ab	11.9	57.6	72.3	48.1	56.0
An	0.7	1.9	3.2	17.4	6.9
Or	87.3	40.5	24.5	34.4	37.1

-Nb anomalies. Their pattern shows pronounced troughs at P and Ti (Fig. 7b).

The metabasaltic andesites, meta-andesites and metadacites of the lower Zaghra unit are enriched in LREE, with (La/Yb)_N ratio of 10–12, (La/Sm)_N ratio of 2.5–4.7, and a nearly flat HREE pattern, with (Gd/Yb)_N ratio of 1.4–2.2 (Fig. 7c). The ΣREE content of basaltic andesites and andesites (aver. 119 ppm) is lower than that of dacites (aver. 132 ppm). In the chondrite-normalized plot of the analyzed lower volcanics show negligible negative Eu anomalies (Eu/Eu* = 0.86–1.08).

The dacites and rhyolites of the upper Zaghra unit are highly fractionated and display similar patterns with LREE enrichment and with flat HREE pattern (Fig. 7d).

They have (La/Yb)_N ratio of 6.4–11.75 and (Gd/Yb)_N ratio of 1.1–1.7. The dacites have small negative anomalies (Eu/Eu* = 0.84–0.88). In rhyolites, the Eu/Eu* ratio is 0.61–0.33, and is 0.16 in high silica rhyolites.

The contents of the selected trace elements have been used to discriminate between different tectonic regimes. Gorton and Schandl (2000) used a plot of Th/Ta versus Yb to discriminate between the tectonic settings for arc-related and within-plate felsic to intermediate volcanic rocks. Figure 8 is such a plot and shows that the metavolcanics of the Zaghra lower unit and the volcanics of the upper unit all lie in the field of Active Continental Margins. Gorton and Schandl (2000) pointed out that Ta, Th and Yb are considered to be immobile under most geological conditions and the Ta/Yb–Th/Yb values are expected to remain constant during metamorphism.

The metasedimentary rocks: The chemical composition of the metasedimentary rocks interbedded with the metavolcanics of the Zaghra lower unit is given in Table 12. The geochemistry of these rocks depends on several variables, such as the nature of the source rocks, metamorphism and tectonic setting of their sedimentary basins.

The major elements of the metasedimentary rocks exhibit two main populations: pelites and graywackes, as shown in Fig. 9a, which is a plot of SiO₂/Al₂O₃ against Na₂O/K₂O, after Wimmenauer (1984).

In general, the metagraywackes contain lower contents of REE than the metapelites. This is expected since the metagraywackes contain more quartz known to contain very low abundances of REE. The pre-existing graywackes, represent the major source of the studied metagraywackes, are rich in plagioclase (Ali Bik et al., 2017), known to have Eu/Eu* of ~1.0 that can reach 1.5 (Bhatia, 1985; McLennan, 1989).

The average of most major elements in the analyzed metapelites is higher than the average of the upper continental crust (UCC); the average of trace elements is

Table 7 Representative microprobe analyses (wt%) of plagioclase feldspars for dacite, Zaghra upper unit

Points	41	42	43	44	45	46	47	48	49	50	51	52	53	54
SiO ₂	62.95	62.98	62.02	65.84	63.82	62.40	62.04	64.33	64.17	61.14	64.02	65.74	65.73	64.85
TiO ₂	0.01	0.02	0.01	0.00	0.00	0.00	0.01	0.00	0.01	0.02	0.01	0.01	0.01	0.01
Al ₂ O ₃	22.48	22.21	22.96	20.05	21.14	22.73	22.95	21.32	21.15	22.73	21.24	20.36	20.53	20.61
FeO	0.11	0.11	0.18	0.02	0.11	0.16	0.15	0.11	0.12	0.47	0.42	0.10	0.08	0.13
MnO	0.01	0.00	0.00	0.00	0.00	0.00	0.00	0.00	0.00	0.01	0.02	0.00	0.00	0.00
MgO	0.00	0.00	0.00	0.00	0.00	0.00	0.00	0.00	0.00	0.23	0.23	0.03	0.00	0.02
CaO	3.73	4.02	4.45	0.67	2.48	4.15	4.59	4.32	3.48	3.95	2.15	1.03	1.39	1.39
Na ₂ O	9.32	9.17	8.80	11.69	10.28	8.54	8.75	8.78	8.22	9.77	10.74	11.67	11.49	10.89
K ₂ O	0.19	0.17	0.32	0.09	0.37	0.13	0.32	0.35	1.68	0.33	0.17	0.20	0.07	0.85
Total	98.80	98.68	98.74	98.36	98.2	98.11	98.81	99.21	98.83	98.65	99.00	99.14	99.30	98.75
Number of cations on the basis of 32 oxygens														
Si	11.258	11.282	11.130	11.753	11.476	11.221	11.128	11.448	11.495	11.043	11.436	11.677	11.652	11.599
Ti	0.002	0.002	0.001	0.000	0.000	0.000	0.001	0.000	0.002	0.003	0.002	0.001	0.001	0.001
Al	4.735	4.685	4.853	4.214	4.476	4.814	4.848	4.467	4.462	4.834	4.468	4.258	4.287	4.343
Fe ³⁺	0.017	0.016	0.027	0.003	0.017	0.024	0.023	0.017	0.018	0.071	0.062	0.015	0.012	0.020
Mn	0.000	0.000	0.000	0.000	0.000	0.000	0.000	0.000	0.000	0.001	0.003	0.000	0.000	0.000
Mg	0.000	0.000	0.000	0.000	0.000	0.001	0.000	0.001	0.001	0.063	0.060	0.008	0.000	0.006
Ca	0.715	0.771	0.855	0.129	0.477	0.799	0.882	0.824	0.669	0.765	0.412	0.195	0.264	0.266
Na	3.233	3.185	3.063	4.047	3.585	2.978	3.042	3.030	2.853	3.421	3.719	4.019	3.949	3.778
K	0.043	0.038	0.074	0.021	0.085	0.031	0.073	0.080	0.384	0.076	0.040	0.045	0.017	0.195
Total	20.003	19.979	20.003	20.167	20.116	19.868	19.997	19.867	19.884	20.277	20.202	20.218	20.182	20.208
Ab	81.0	79.7	76.7	96.4	86.4	78.2	76.1	77.0	73.0	80.3	89.2	94.4	93.4	89.1
An	17.9	19.3	21.4	3.1	11.5	21.0	22.1	20.9	17.1	17.9	9.9	4.6	6.2	6.3
Or	1.1	1.0	1.9	0.5	2.0	0.8	1.8	2.0	9.8	1.8	1.0	1.1	0.4	4.6

Table 8 Representative microprobe analyses (wt%) of plagioclase and alkali feldspars for rhyolite Zaghra upper unit

Points	Plagioclases			K-feldspars							K-feldspars					
	60	61	62	63	64	65	66	67	68	69	70	71	72	73	74	75
SiO ₂	68.71	69.56	70.02	68.71	65.66	66.22	65.15	66.06	66.09	64.9	65.44	65.53	65.84	66.92	64.75	67.94
TiO ₂	0.00	0.00	0.00	0.00	0.01	0.01	0.03	0.02	0.00	0.02	0.02	0.04	0.01	0.00	0.01	0.00
Al ₂ O ₃	19.54	20.17	20.42	19.62	18.66	18.67	18.52	19.05	18.81	18.47	18.47	18.56	18.7	18.65	18.56	19.14
FeO	0.02	0.07	0.39	0.00	0.05	0.02	0.1	0.00	0.03	0.04	0.03	0.04	0.04	0.03	0.00	0.01
MnO	0.00	0.00	0.00	0.00	0.00	0.01	0.00	0.00	0.00	0.01	0.01	0.01	0.00	0.00	0.00	0.03
MgO	0.00	0.00	0.02	0.00	0.00	0.00	0.01	0.01	0.01	0.00	0.02	0.01	0.01	0.00	0.00	0.01
CaO	0.33	0.13	0.12	0.28	0.00	0.00	0.00	0.09	0.00	0.00	0.09	0.11	0.00	0.00	0.00	0.01
Na ₂ O	10.29	9.01	9.15	9.03	0.3	0.33	0.24	0.35	0.38	0.40	0.85	0.75	0.38	0.62	0.26	4.24
K ₂ O	0.18	0.10	0.06	1.85	15.69	15.7	15.73	14.86	15.79	15.59	15.15	15.22	15.46	14.45	16.01	8.8
Total	99.07	99.04	100.18	99.49	100.37	100.96	99.78	100.44	101.11	99.43	100.08	100.27	100.44	100.67	99.59	100.18
Number of cations on the basis of 32 oxygens																
Si	12.052	12.112	12.078	12.058	12.028	12.050	12.019	12.027	12.021	12.015	12.020	12.014	12.037	12.122	11.990	12.112
Ti	0.000	0.000	0.000	0.000	0.002	0.002	0.004	0.003	0.000	0.002	0.003	0.006	0.002	0.000	0.002	0.000
Al	4.036	4.135	4.147	4.055	4.027	4.002	4.024	4.084	4.029	4.026	3.995	4.007	4.025	3.977	4.048	4.019
Fe ²⁺	0.003	0.011	0.056	0.000	0.007	0.004	0.015	0.000	0.005	0.006	0.005	0.006	0.006	0.004	0.000	0.002
Mn	0.000	0.000	0.000	0.000	0.000	0.001	0.000	0.000	0.001	0.002	0.002	0.002	0.000	0.000	0.000	0.004
Mg	0.000	0.000	0.005	0.000	0.001	0.001	0.003	0.003	0.002	0.001	0.005	0.003	0.001	0.000	0.000	0.001
Ca	0.062	0.024	0.022	0.053	0.000	0.000	0.000	0.018	0.000	0.000	0.018	0.022	0.000	0.000	0.000	0.002
Na	3.500	3.043	3.059	3.073	0.107	0.118	0.086	0.124	0.135	0.144	0.303	0.267	0.136	0.219	0.094	1.464
K	0.040	0.023	0.012	0.414	3.668	3.645	3.702	3.451	3.664	3.682	3.550	3.560	3.605	3.340	3.782	2.002
Total	19.693	19.348	19.379	19.653	19.840	19.823	19.853	19.710	19.857	19.878	19.901	19.887	19.812	19.662	19.916	19.606
Ab	97.2	98.5	98.9	86.8	2.80	3.1	2.3	3.5	3.6	3.8	7.8	6.9	3.6	6.2	2.4	42.2
An	1.7	0.8	0.7	1.5	0.0	0.0	0.0	0.5	0.0	0.0	0.5	0.6	0.0	0.0	0.0	0.1
Or	1.1	0.7	0.4	11.7	97.2	96.9	97.7	96.0	96.4	96.2	91.7	92.5	96.4	93.8	97.6	57.7

either higher or comparable to the UCC. The metagraywackes have lower or comparable contents of major and trace elements to those of the UCC (Rudnick and Gao, 2003). The metapelites contain similar value of total REE (aver. 139 ppm) as the UCC (aver. 146 ppm), whereas metagraywackes have lower contents (92 ppm). Both metapelites and metagraywackes have higher Eu contents (1.13–1.77 ppm) and Eu anomalies ($\text{Eu}/\text{Eu}^* = 0.98$ –1.15) than those of the UCC with $\text{Eu} = 0.88$ ppm and $\text{Eu}/\text{Eu}^* = 0.65$ (Taylor and McLennan, 1985).

The provenance of the investigated metasedimentary rocks can be assessed using the ACF diagram (Fig. 9b). They plot outside the field of the igneous protolith, which is delimited by the clinopyroxene, labradorite and olivine

and orthopyroxene reference points, indicating their formation through erosion, transportation and sedimentation processes of pre-existing sedimentary rocks.

The tectonic setting of sedimentary basins or of source areas has been considered as the overall primary control on the composition of clastic sedimentary rocks (Bhatia and Crook, 1986; McLennan and Taylor, 1991; Roser and Korsch, 1999). It is agreed that the framework grains of sandstones are liable to be modified by post-depositional processes. Upon metamorphism, the nature of the grains can be destroyed and the larger part of the matrix can have been formed by degradation of lithic grains and therefore modal composition cannot always be used to infer tectonic settings (Bhatia, 1983; McLennan and Taylor, 1991). Thus,

Table 9 Representative microprobe analyses (wt%) of amphiboles and pyroxenes of Wadi Zaghra volcanics

Rock type	Andesite (Lower Unit)					Dacite (Upper Unit)			Andesite (Lower Unit)						
	Primary amphiboles		Secondary amphiboles			Primary amphiboles			Pyroxenes						
Points	1	2	3	4	5	6	7	1	2	3	4	5	6	7	8
SiO ₂	42.56	48.28	48.53	49.21	49.24	44.10	44.22	48.06	53.23	49.84	50.61	51.58	48.71	48.97	49.61
TiO ₂	1.91	0.51	0.44	0.38	0.38	2.13	2.11	1.69	1.32	1.31	1.03	0.99	1.93	1.79	1.51
Al ₂ O ₃	9.01	5.08	5.02	4.34	4.23	8.60	8.31	3.62	1.84	2.56	1.81	1.77	3.56	3.46	2.68
FeO	17.91	14.51	14.55	14.08	13.33	15.44	15.49	11.39	10.91	11.70	11.85	11.72	12.20	11.71	13.07
MnO	1.19	1.11	1.16	1.18	1.12	0.20	0.20	0.28	0.33	0.32	0.36	0.38	0.33	0.35	0.40
MgO	10.03	13.89	13.65	13.81	13.22	12.00	12.11	13.22	13.69	13.34	14.85	14.52	13.35	13.40	13.35
CaO	11.38	10.27	10.90	12.19	11.85	11.00	11.29	19.41	19.01	18.67	17.95	18.36	18.24	18.81	17.63
Na ₂ O	1.27	0.38	0.46	0.54	0.79	1.64	1.81	0.46	0.43	0.38	0.36	0.37	0.38	0.43	0.43
K ₂ O	0.71	1.34	0.87	0.25	0.25	0.91	0.80	0.00	0.00	0.00	0.01	0.00	0.00	0.00	0.00
Total	95.97	95.37	95.58	95.98	94.41	96.02	96.34	98.13	100.76	98.12	98.83	99.69	98.70	98.92	98.68
Number of cations on the basis of 23 oxygens								Number of cations on the basis of 6 oxygens							
Si	6.499	7.190	7.216	7.290	7.439	6.657	6.667	1.834	1.982	1.907	1.912	1.936	1.855	1.857	1.893
Al ^{IV}	1.501	0.799	0.784	0.710	0.561	1.343	1.333	0.163	0.018	0.093	0.080	0.064	0.145	0.143	0.107
Al ^{VI}	0.119	0.093	0.095	0.046	0.191	0.186	0.143	0.000	0.063	0.022	0.000	0.014	0.014	0.012	0.013
Ti	0.220	0.057	0.049	0.042	0.043	0.242	0.239	0.049	0.037	0.038	0.029	0.028	0.055	0.051	0.043
Fe ³⁺	0.573	0.632	0.572	0.449	0.115	0.307	0.252	0.105	0.000	0.023	0.063	0.021	0.048	0.060	0.039
Fe ²⁺	1.714	1.175	1.237	1.296	1.569	1.643	1.701	0.258	0.339	0.352	0.312	0.347	0.340	0.311	0.378
Mn	0.153	0.140	0.145	0.148	0.143	0.026	0.026	0.009	0.010	0.010	0.012	0.012	0.011	0.011	0.013
Mg	2.284	3.084	3.025	3.049	2.977	2.701	2.721	0.752	0.760	0.761	0.837	0.812	0.757	0.758	0.759
Ca	1.862	1.639	1.736	1.935	1.917	1.779	1.824	0.794	0.758	0.765	0.727	0.738	0.744	0.764	0.721
Na	0.377	0.111	0.134	0.154	0.230	0.481	0.530	0.034	0.031	0.028	0.027	0.027	0.028	0.031	0.032
K	0.139	0.254	0.165	0.046	0.049	0.175	0.154	0.000	0.000	0.000	0.001	0.000	0.000	0.000	0.000
Total	15.441	15.174	15.158	15.165	15.234	15.540	15.590	3.998	3.998	3.999	4.000	3.999	3.997	3.998	3.998
Wo								41.4	40.6	40.0	37.3	38.2	39.1	40.2	37.7
En								39.2	40.7	39.8	42.9	42.1	39.9	39.8	39.8
Fs								19.4	18.7	20.1	19.8	19.7	21.0	20.1	22.5

Table 10 Representative microprobe analyses (wt%) of biotites for metadacite, Zaghra lower unit

Points	1	2	3	4	5	6	7	8	9	10	11	12	13	14	15	16	17
SiO ₂	34.61	44.91	36.16	25.83	35.17	35.72	35.18	35.98	35.04	32.71	34.95	36.20	36.11	36.62	36.36	36.55	36.05
TiO ₂	2.53	1.92	2.51	2.56	3.07	3.19	2.94	2.89	2.80	2.50	2.66	3.30	3.60	3.42	3.34	3.16	2.71
Al ₂ O ₃	15.12	17.42	15.24	12.56	14.82	15.16	15.24	15.13	14.98	14.58	15.30	15.02	14.87	15.05	14.74	14.71	15.47
FeO	18.21	11.84	17.53	16.27	17.31	17.23	17.37	17.44	17.35	16.76	17.31	17.24	17.58	16.70	16.98	17.13	17.53
MnO	0.55	0.39	0.54	0.56	0.57	0.61	0.59	0.57	0.58	0.59	0.56	0.63	0.58	0.59	0.63	0.61	0.56
MgO	12.35	7.92	11.64	12.24	11.39	11.26	11.83	11.37	11.67	12.26	12.71	11.76	11.52	11.66	11.86	11.98	11.91
CaO	0.04	1.04	0.04	0.07	0.09	0.16	0.04	0.08	0.10	0.20	0.15	0.03	0.03	0.04	0.05	0.01	0.09
Na ₂ O	0.07	3.07	0.06	0.10	0.18	0.08	0.12	0.14	0.15	0.13	0.08	0.11	0.12	0.14	0.13	0.11	0.07
K ₂ O	8.48	7.34	9.78	8.33	8.99	9.55	9.52	9.29	8.97	8.87	8.73	9.42	9.19	9.24	9.21	9.05	8.69
Total	91.96	95.85	93.50	78.52	91.59	92.96	92.83	92.89	91.64	88.60	92.45	93.71	93.60	93.46	93.30	93.31	93.08
Number of cations on the basis of 22 oxygens																	
Si	5.710	6.693	5.864	5.142	5.814	5.800	5.754	5.860	5.792	5.625	5.715	5.841	5.837	5.893	5.877	5.902	5.833
Al ^{IV}	2.290	1.307	2.136	2.858	2.186	2.200	2.246	2.140	2.208	2.375	2.285	2.159	2.163	2.107	2.123	2.098	2.167
Al ^{VI}	0.648	1.750	0.775	0.087	0.700	0.699	0.689	0.762	0.708	0.578	0.661	0.694	0.667	0.745	0.683	0.698	0.781
Ti	0.315	0.216	0.306	0.383	0.382	0.389	0.362	0.354	0.348	0.323	0.327	0.401	0.437	0.414	0.406	0.384	0.330
Fe ³⁺	2.513	1.475	2.376	2.709	2.394	2.340	2.375	2.376	2.398	2.410	2.367	2.326	2.377	2.248	2.296	2.313	2.373
Mn	0.077	0.050	0.074	0.095	0.080	0.084	0.082	0.078	0.081	0.085	0.078	0.086	0.079	0.080	0.086	0.083	0.077
Mg	3.039	1.760	2.813	3.634	2.808	2.814	2.884	2.760	2.876	3.144	3.098	2.828	2.776	2.798	2.859	2.884	2.873
Ca	0.008	0.166	0.007	0.015	0.015	0.029	0.007	0.014	0.017	0.036	0.026	0.005	0.005	0.007	0.010	0.001	0.016
Na	0.022	0.886	0.019	0.037	0.059	0.026	0.039	0.043	0.049	0.042	0.025	0.035	0.038	0.045	0.040	0.035	0.023
K	1.786	1.396	2.022	2.115	1.896	1.978	1.986	1.929	1.891	1.945	1.822	1.940	1.894	1.897	1.900	1.864	1.794
Total	16.408	15.699	16.392	17.075	16.334	16.359	16.424	16.316	16.368	16.563	16.404	16.315	16.273	16.234	16.280	16.262	16.267

the geochemical characteristics of clastic sedimentary rocks, including sandstones and mudstones metamorphosed up to lower amphibolite facies, can effectively be used to evaluate their tectonic setting (Bhatia, 1983; Roser and Korsch, 1988, McLennan and Taylor, 1991). The SiO₂, K₂O and Na₂O contents (recalculated on dry basis) of the investigated metagraywackes fall mostly in the field of the active continental margin (ACM) on the diagram proposed by Roser and Korsch (1986) (Fig. 9c). However, the two samples of metapelites plot in the field of an oceanic island arc (OIA). The latter are expected to be derived

from the island arc sediments located to the north of Wadi Zaghra (meta-sedimentary Ra'ayan Formation). These are compatible with the age of zircon grains from the biotite schists, considered to be developed under greenschist facies conditions of pelitic units, having the most pronounced peaks at 650–700 Ma and 800 Ma (Andresen et al., 2014). On the FI-FII discriminant diagram of Bhatia (1983; Fig. 9d), the metagraywackes fall either in the ACM field or continental island arc (CIA).

The concentration of some trace elements and some elemental ratios can be used to differentiate between marine and freshwater environments of fine clastic

Table 11 Representative microprobe analyses (wt%) of biotites for dacite, Zaghra upper unit

Points	18	19	20	21	22	23
SiO ₂	34.52	34.75	34.22	36.24	35.87	35.54
TiO ₂	5.00	4.56	5.44	3.25	3.15	3.32
Al ₂ O ₃	13.85	14.02	13.95	13.71	13.62	13.46
FeO	21.02	20.35	20.67	21.56	21.42	21.42
MnO	0.30	0.36	0.29	0.43	0.44	0.38
MgO	10.84	11.66	11.74	10.95	11.02	10.98
CaO	0.48	0.76	1.43	0.07	0.04	0.04
Na ₂ O	0.17	0.15	0.07	0.08	0.06	0.06
K ₂ O	8.02	6.92	6.26	8.98	9.05	9.26
Total	94.20	93.53	94.07	95.27	94.67	94.46
Number of cations on the basis of 22 oxygens						
Si	5.637	5.660	5.545	5.861	5.844	5.819
Al ^{IV}	2.363	2.340	2.455	2.139	2.156	2.181
Al ^{VI}	0.301	0.349	0.208	0.473	0.458	0.413
Ti	0.614	0.558	0.663	0.395	0.386	0.409
Fe ²⁺	2.871	2.771	2.802	2.917	2.919	2.933
Mn	0.042	0.050	0.039	0.058	0.061	0.053
Mg	2.638	2.830	2.837	2.640	2.677	2.680
Ca	0.084	0.132	0.249	0.012	0.008	0.007
Na	0.054	0.049	0.021	0.024	0.020	0.018
K	1.672	1.439	1.294	1.854	1.880	1.933
Total	16.276	16.178	16.113	16.373	16.409	16.446

sediments, respectively. According to Potter et al. (1963), the average MnO content is 0.80% and 0.12% for marine and freshwater shales, respectively. The average content of MnO in the studied metagraywackes is 0.09% and in the metapelites is 0.21%, indicating their general freshwater environment. High Rb/K ratio (>0.006) and low values (<0.004) are given by Campbell and Williams (1965) for marine and freshwater environments of fine clastic sediments. The analyzed metasediments have an Rb/K ratio that varies from 0.0015 to 0.0053, with an average of 0.0039, substantiating their freshwater environment.

Andresen et al. (2014) speculated that the island arc Agramyia and Ra'ayan Formations were separated from the Zaghra Formation (a time gap of about 400 Ma between both, Eyal et al., 2013) by an extensional shear zone and that the latter was deposited in grabens by the rider faults of this zone. The studied metasediments are most probably related to the late orogenic molasse facies sediments. The latter are largely coarse terrigenous clastics with abundant conglomerates and negligible limestones. These sediments were laid down in non-marine fluvial and fanglomerate environments. They accumulated in intermontane basins frequently in the form of half grabens or tilted fault blocks in which the conglomerates accumulate near the border fault (cf. Grothaus et al., 1979; Ries et al., 1983; El-Gaby, 2007). In the ED, Abu El-Ela and El Bahariya (1997) divided the Hammamat Molasse sediment into: (1) normal Hammamat, (2) tectonized Hammamat, and (3) metamorphosed tectonized Hammamat. The studied Hammamat sediments of Wadi Zaghra are comparable with the metamorphosed tectonized Hammamat sediments in Wadi Um Esh and Wadi Muweilih in the central ED (Abu El-Ela and El Bahariya, 1997).

5.3 Discussion

As noted above, the Zaghra succession is divided into

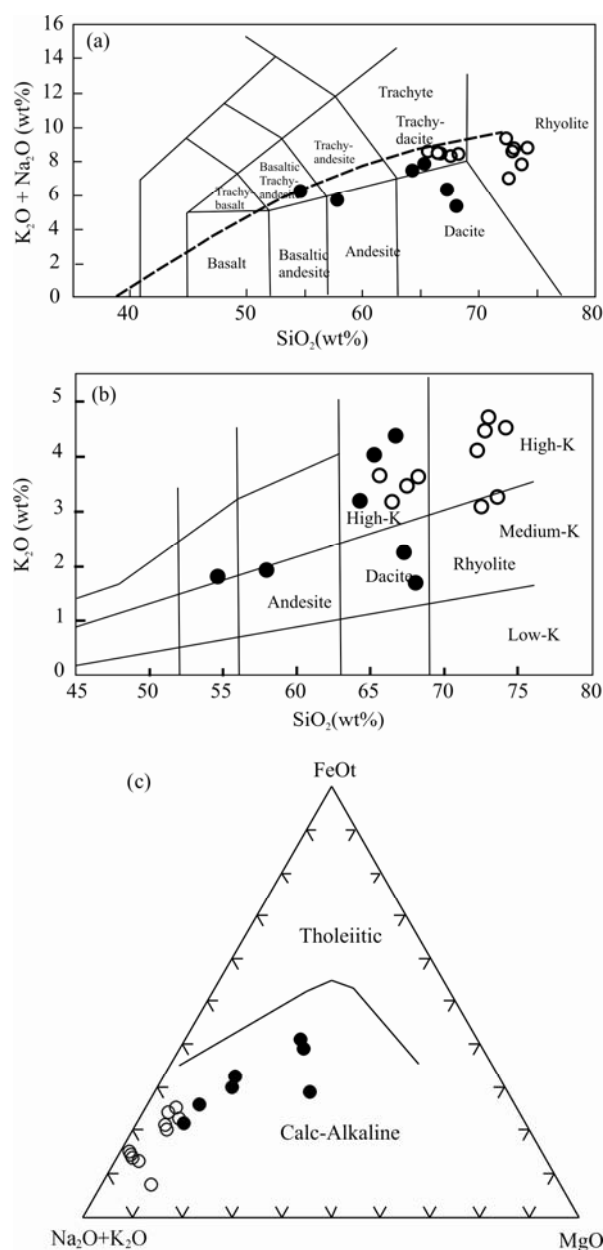


Fig. 5. (a), TAS classification diagram for Zaghra volcanics (Le Maitre, 2002). ● = lower volcanic unit; ○ = upper volcanic unit. Separating line after Irvine and Baragar (1971); (b), SiO₂ vs. K₂O classification diagram with the boundary lines after Ewart (1982); (c), AFM diagram showing distinction between tholeiitic and calc-alkaline suites (Irvine and Baragar, 1971).

lower and upper units including volcanics interbedded with rather immature sediments separated by a major unconformity represented by the metaconglomerates deposited during 625–615 Ma (Andresen et al., 2014). The lower part is metamorphosed with pronounced foliation implying the beginning of a tectonic phase marked by onset of thrusting, folding and volcanicity. The succession is folded into a major syncline trending NE–SW and is bounded by many faults (Shimron et al., 1993; Mehanna et al., 2001; El-Gaby et al., 2002). The succession has

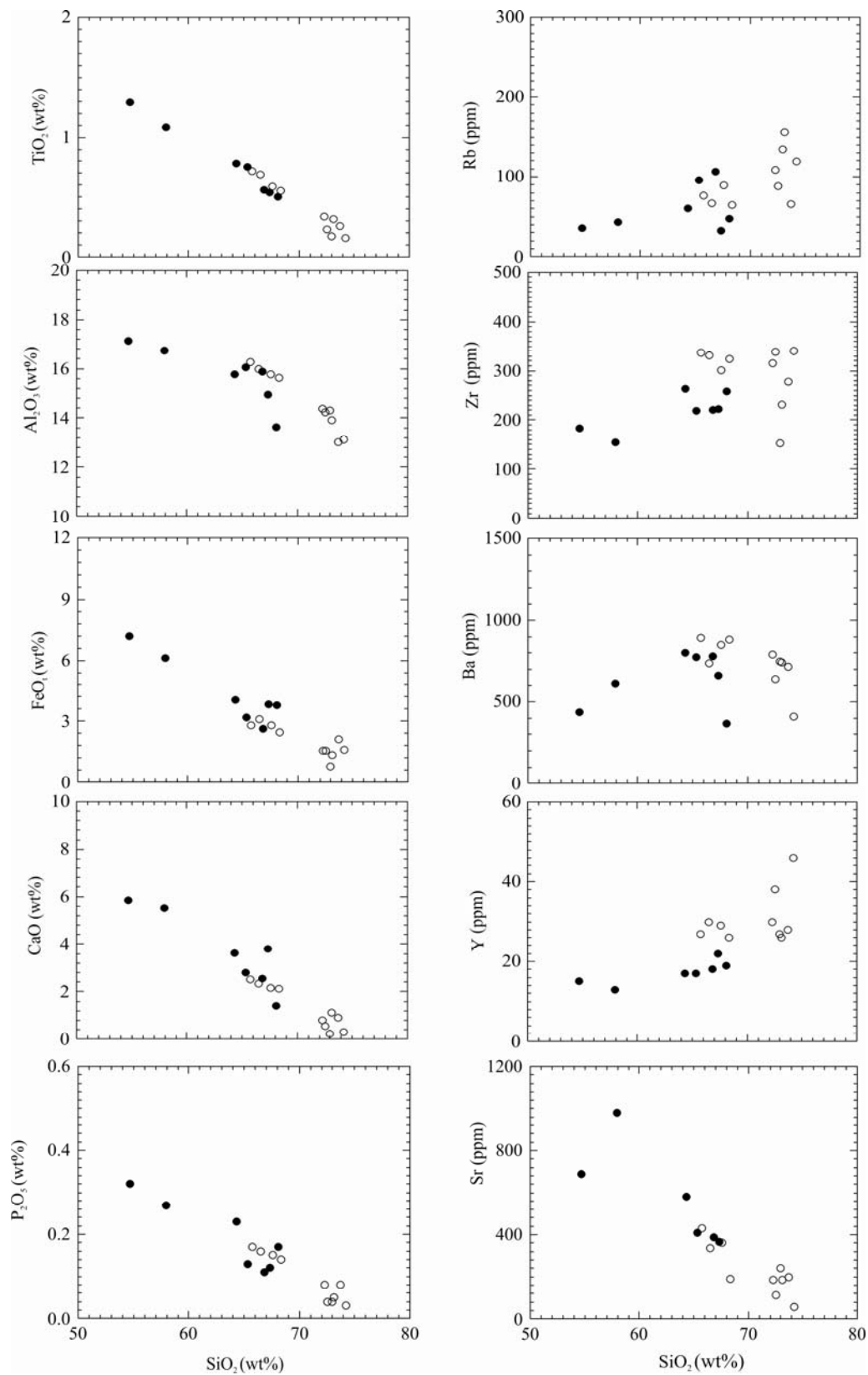


Fig. 6. Harker variation diagrams of some major and trace elements in the volcanics of the Zaghra area; symbols as in Fig. 5.

been subjected to low pressure regional metamorphism not attributed to an outcropping granite intrusion, although some samples are incorporated in a low pressure thermal

aureole, which would suggest an igneous body at depth. The recognized major unconformity represents major uplift and an erosional phase after the lower Zaghra unit

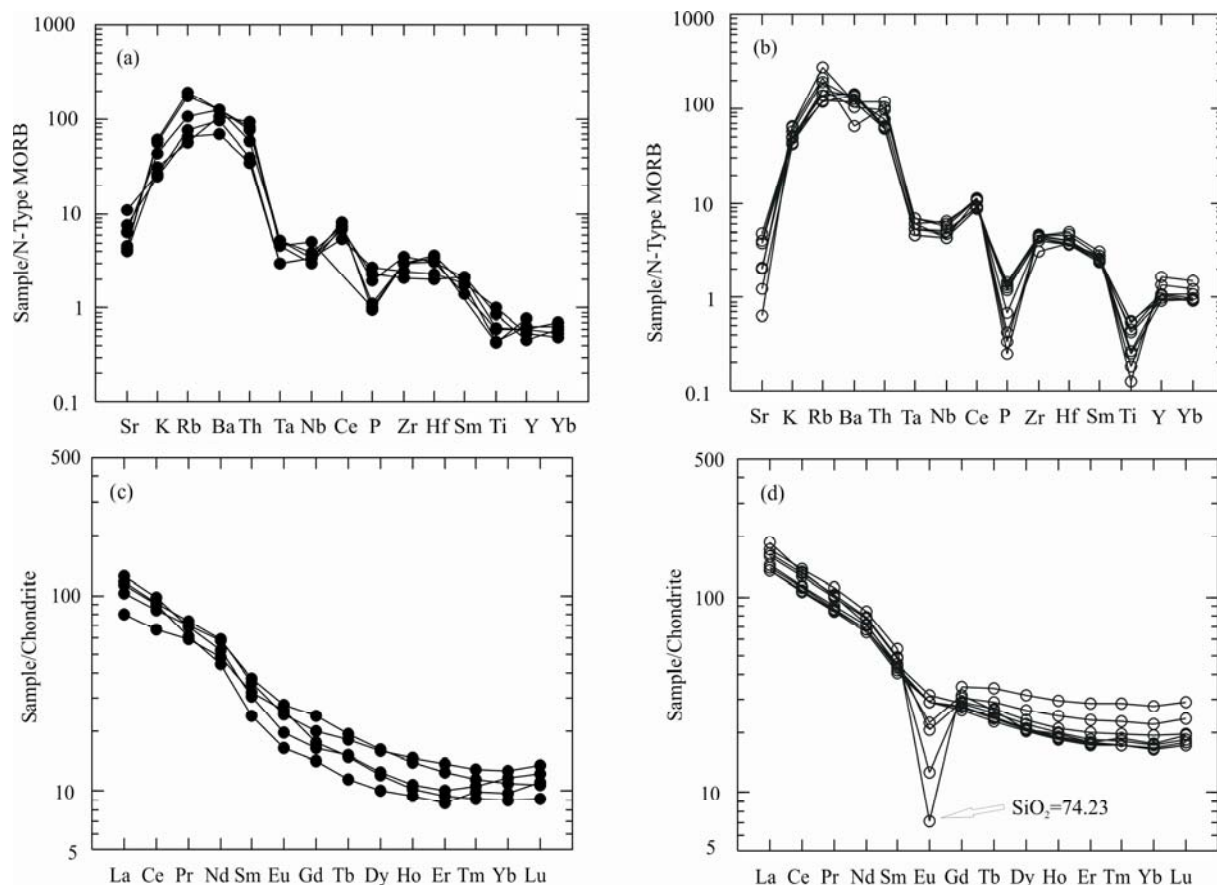


Fig. 7. MORB-normalized trace element plots and chondrite-normalized patterns for the Zaghra volcanics. (a) and (c) are Lower Zaghra; (b) and (d) are Upper Zaghra; symbols as in Fig. 5.

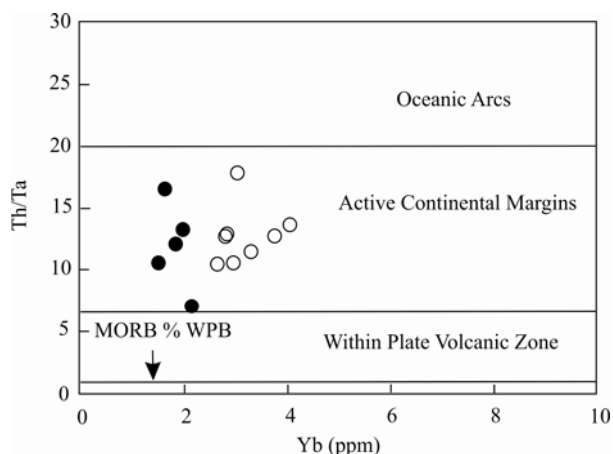


Fig. 8. Tectonic setting diagram for the Zaghra volcanics (after Gorton and Schandl, 2000); symbols as in Fig. 5.

and contemporaneous igneous intrusion, which predates the second phase of volcanism and sediment deposition constituting the upper unit that includes unmetamorphosed volcanics interbedded with sediments. The Zaghra succession has been intruded by monzogranite and alkali-feldspar granite.

5.3.1 Magma sources and petrogenesis of Zaghra volcanics

The petrographic, mineralogical and geochemical

characteristics of the Wadi Zaghra volcanics described here indicate an ACM calc-alkaline series (basaltic andesite–andesite–dacite–rhyolite). The fact that the lower Zaghra unit volcanics are represented by this series, and those in the upper unit by dacite–rhyolite, might suggest that there were two episodes of eruptions of the same calc-alkaline series, separated by the conglomerate. El-Gaby (2007) suggested that the differences in the volcanics related to a Neoproterozoic subduction related- calc-alkaline magma series divided into a lower and an upper Dokhan series separated by an hiatus. The data obtained in the present work indicate that there is no substantial geochemical difference between the lower and upper Zaghra dacites although those of the lower unit are metamorphosed. Age determination of both dacites is in progress to clarify this issue.

The Zaghra volcanics are enriched in most LILE (K, Rb, Ba) and Th and depleted in P and Ti, with clear Nb-Ta anomalies. This pattern is typical for calc-alkaline subduction-related magmas (Condie, 1989; Hawkesworth et al., 1993). Moreover, the silicic volcanics (SiO_2 wt% > 63) of both units plot in the volcanic-arc granite field (VAG) on the Ta–Yb diagram of Pearce et al. (1984) (Fig. 10). However, in Whalen et al.'s (1987) classification diagrams ($10,000 \times \text{Ga}/\text{Al}$ vs. Ce, Nb, Zr and Y), the rhyolites would plot either in the A-type granite field or near its boundary with the I-type field (Fig. 11). The volcanics have an agpaitic index $0.87 > \text{NK}/\text{A} < 1.0$ (i.e.

Table 12 Major oxides (wt%) and trace elements (ppm) of the studied metasedimentary rocks

Rock type	Lower metagreywackes								Lower metapelites		
Sample No.	1	19	25	30	20	35	Kh-2A	Kh-3	Kh-7	40	Kh-2
SiO ₂	74.19	63.25	67.76	66.24	74.41	72.54	76.12	73.91	70.43	51.30	54.39
TiO ₂	0.29	0.87	0.61	0.69	0.07	0.09	0.35	0.29	0.49	1.26	1.46
Al ₂ O ₃	12.96	16.50	14.20	14.51	13.93	14.81	11.37	13.24	13.54	16.93	15.36
Fe ₂ O ₃	2.50	8.81	4.87	5.57	0.71	1.42	2.77	2.51	3.88	7.71	8.61
MnO	0.06	0.14	0.10	0.10	0.06	0.10	0.06	0.07	0.11	0.26	0.15
MgO	0.91	1.82	3.22	3.16	0.87	1.34	1.61	0.82	1.37	6.01	5.16
CaO	0.70	2.52	1.83	1.95	0.23	0.50	0.66	0.81	0.79	6.80	5.43
Na ₂ O	3.44	1.83	3.24	3.20	4.26	4.61	2.76	2.41	4.98	4.16	4.54
K ₂ O	3.33	2.20	1.86	1.84	3.43	2.48	2.38	3.83	2.26	2.43	1.37
P ₂ O ₅	0.08	0.19	0.13	0.15	0.06	0.08	0.08	0.08	0.13	0.43	0.51
Total	98.46	98.13	97.82	97.41	98.03	97.97	98.16	97.97	97.98	97.29	96.98
Ba	781	287	457	528	760	740	502	706	628	345	1036
Co	5	16	11	14	4	4	8	9	4	30	23
Cr	0	62	30	49		0	0	0	0	104	226
Cu	35	30	21	23	59	149	47	51	42	6	60
Nb	9	9	8	7	14	11	8	10	10	11	8
Ni	13	43	25	27	3	15	12	8	10	61	64
Pb	110	8	24	19	36	50	30	75	16	16	12
Rb	105	97	53	55	102	83	94	136	62	106	48
Sr	184	223	281	504	223	425	434	287	537	401	1037
Th	18	12	9	11	4	9	8	9	15	7	9
V	24	128	78	102	0	10	32	18	44	208	181
Y	28	28	23	20	23	27	31	36	34	27	17
Zr	177	156	134	154	69	135	188	191	214	148	181
Zn	65	118	86	78	37	64	71	73	87	167	141
La			17.8							25.9	26.1
Ce			37.5							54.5	58.2
Pr			4.58							6.77	7.4
Nd			19							28.2	31.7
Sm			4.2							5.82	5.92
Eu			1.13							1.63	1.77
Gd			2.93							3.97	3.72
Tb			0.54							0.65	0.51
Dy			3.74							4.19	2.9
Ho			0.82							0.89	0.54
Er			2.36							2.43	1.38
Tm			0.35							0.33	0.18
Yb			2.27							2.07	1.16
Lu			0.35							0.32	0.17

alkaline) and belong to the highly fractionated granites delineated in the discriminant diagram of Sylvester (1989). These rhyolites with Ta-Nb anomalies may in part refer to a change in the tectonic environment accompanied by change to more alkaline composition and hence represent derivation of magmas from the lithospheric mantle, which has previously been metasomatized by earlier subduction processes (cf. Friz-Töpfer, 1991; Moghazi, 2003; Be'eri-Shlevin et al., 2011). This is evident in the plutonic suites related to post-collisional environment (Stern and Gottfried, 1986; Beyth et al., 1994; Be'eri-Shlevin et al., 2009; Eyal et al., 2010). It is also possible that these rhyolites were formed during extensive interaction of subduction-related magma with the continental crust (cf. El-Gaby et al., 1988; Moussa, 2003).

The present major and trace element geochemical data support the cogenetic relationship of the volcanics of both units (AFM diagram, Fig. 5c). The normalized REE pattern of all volcanic rocks show distinct LREE enrichment and only limited fractionation of HREE, suggesting also the co-magmatic relationship of all members of the Zaghra volcanics. The N-type MORB normalized multi-element diagram for the lower unit volcanics shows Sr, P and Ti depletions in dacites relative to both andesites and basaltic

andesites, referring to fractional crystallization processes. Similarly, the lower volcanic members exhibit similar slope with a general increase of Σ REE for dacites (123–139 ppm) and rather flat HREE patterns [(Gd/Yb)_N=1.42–1.6] with respect to the andesite with Σ REE=132 ppm and (Gd/Yb)_N=2.23. Moreover, the basaltic andesite has lower Σ REE (105 ppm) and higher Eu/Eu* (1.08) in comparison with other volcanics, which might suggest that the intermediate magmas are basaltic differentiates that are genetically related to the andesite–dacite suite.

Plagioclase and amphibole are the main fractionating phases during the crystallization of the basaltic andesite–dacite–dacite. The decrease in the normalized Eu/Eu* from 1.08 to 0.92 and 0.89 coupled with the decrease in CaO (CaO=5.85, 5.51 and 2.84 wt in basaltic andesite, andesite and dacite, respectively) indicate fractionation of the plagioclase. Decreasing of Al₂O₃ with silica up to ~65 wt% and then increase with increasing silica followed by a marked decrease at ~68 wt% SiO₂ can be interpreted to reflect that amphibole is an important additional fractionating phase from basaltic andesite to andesite. Decrease of TiO₂, CaO, FeO, P₂O₅ with increasing SiO₂ coupled with increase in Zr, Y, Nb contents refer to fractionation of the apatite and Fe-Ti oxides.

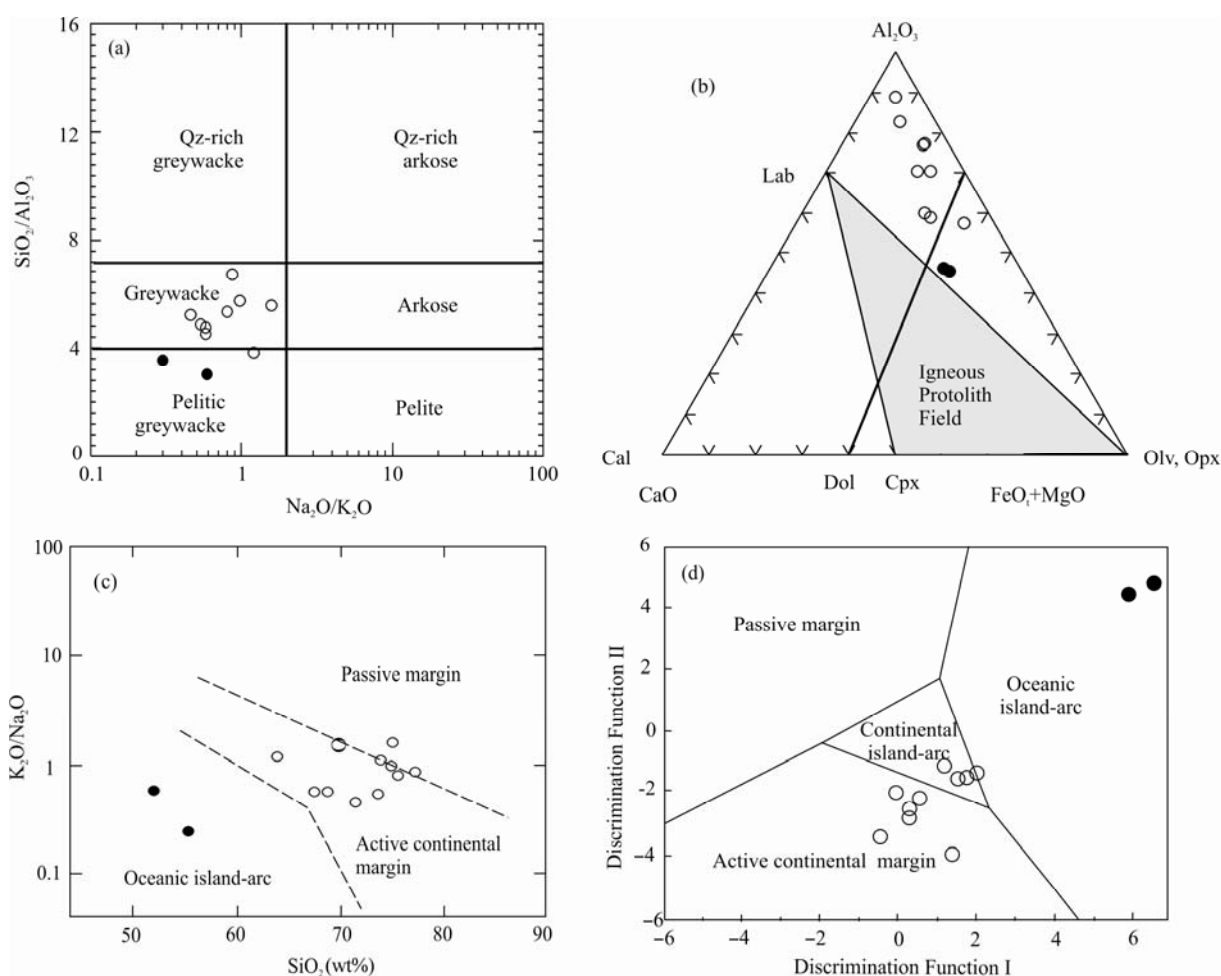


Fig. 9. (a), The chemical classification of the Zaghra metasedimentary rocks according to the diagram of Wimmenauer (1984), (b), ACF provenance diagram (after Dorais et al., 2001) for the chemical composition of the Zaghra metasedimentary rocks, the composition of Lab, Olv, Opx, Cpx, Dol and Cal are given as reference points; (c), K_2O/Na_2O vs. SiO_2 tectonic setting diagram of Roser and Korsch (1986); and (d), FI-FII tectonic setting diagram of Bhatia (1983). ● = lower metapelites; ○ = lower metagraywackes.

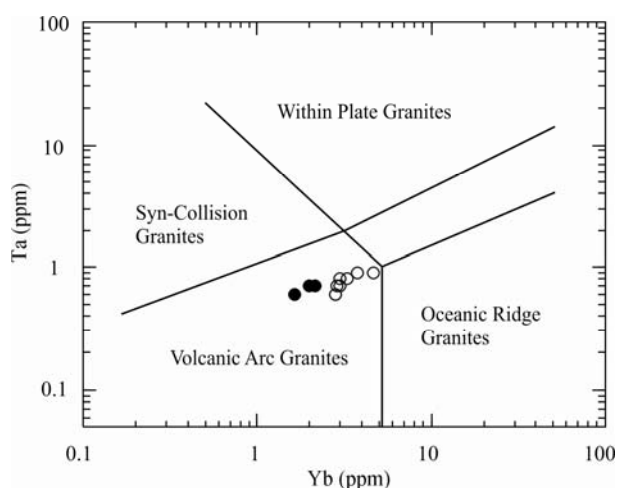


Fig. 10. Ta vs. Yb tectonic discrimination diagram of the Zaghra silicic volcanics (after Pearce et al., 1984); symbols as in Fig. 6.

Dacites of the upper Zaghra unit show similar major and trace element distributions as those of the lower unit but they have higher contents of Zr, Y, Nb, REE although

comparable Eu/Eu^* .

The similarity of the dacites of both units most probably reflects melting from a similar source. The lack of andesites in the upper unit might be attributable to remelting of fractionated magma chambers that formed within the crust during the previous magmatic cycle. This feature was recorded in the upper unit of the comparable Rutig succession (Be'eri-Shlevin et al., 2011).

The N-type MORB normalized multi-element diagram for the rhyolites shows significant Sr, P and Ti depletions and Ba troughs confirming fractional crystallization processes. The rhyolites display similar slopes to the dacites with increased ΣREE (191–213 ppm) and extreme negative Eu anomalies (0.61–0.16) vs. small negative ones in the dacites (0.88–0.84). The remarkable negative Eu anomalies in the rhyolites accompanied by increase of LREE and HREE and decrease in Ca and Sr relative to dacites confirm continuous plagioclase fractionation (Wilson, 1994; Zuo Chen et al., 2005; Li et al., 2017). The continuous Fe, Ti and V depletion from dacite to rhyolite indicates continuous removal of Fe-Ti oxides. The systematic decrease of P and Ca suggests the fractionation

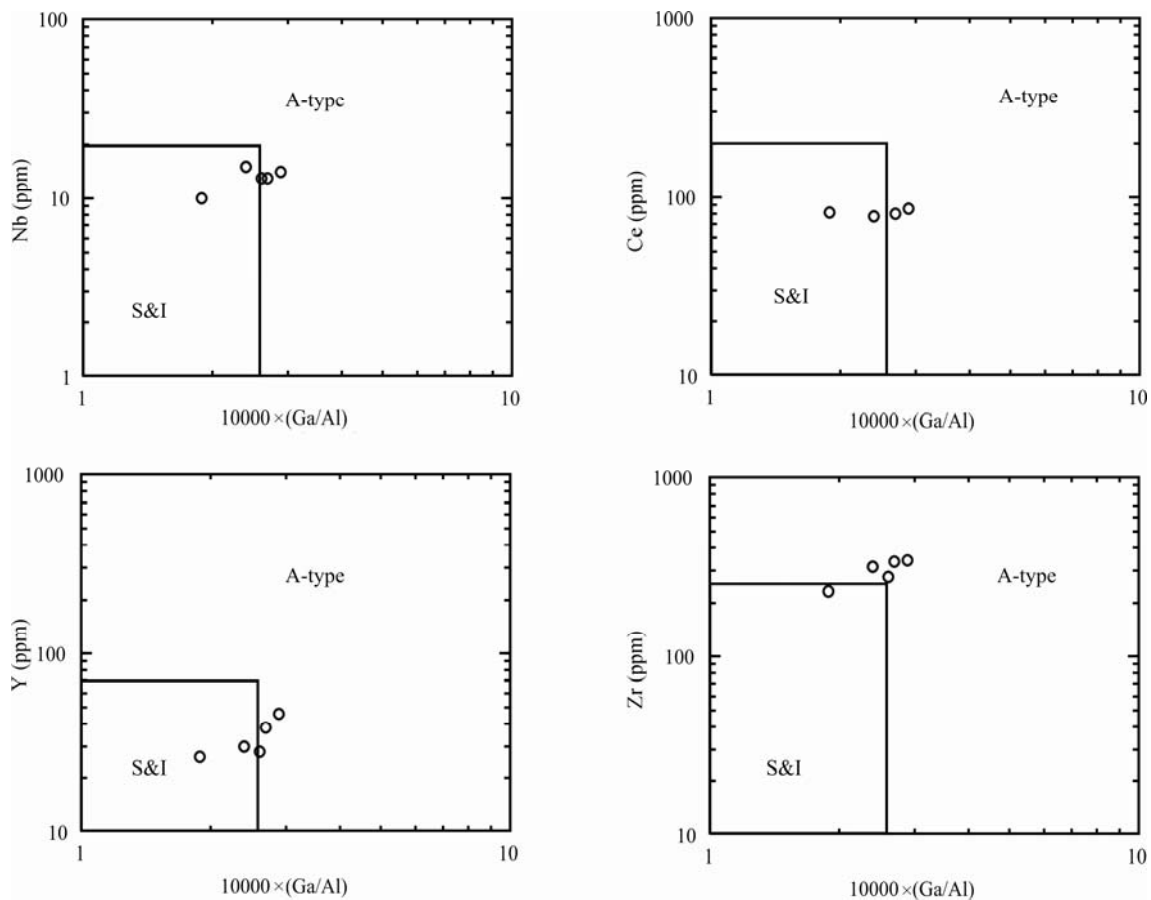


Fig. 11. $10,000 \times \text{Ga}/\text{Al}$ vs. Nb, Ce, Y and Zr classification diagrams after Whalen et al. (1987). \circ = rhyolites of the upper unit.

of apatite. Moreover, alkali feldspars (sanidine and albite) were the dominant fractionating phases within the rhyolites, i.e. from the low-silica rhyolite to the more evolved rhyolite. The depletion in Ba (408 ppm) in the high-silica rhyolite compared to the low-silica rhyolites (an average of 721 ppm) support the idea that alkali feldspars were the main crystallizing phases in this stage. The narrow range of the normalized Ce/Yb (5.08–7.49) confirms low pressure fractional crystallization since this process does not modify the Ce/Yb ratio significantly (Wilson, 1994).

5.3.2 Provenance and tectonic setting of Zaghra Clastics

The conglomerates separating the lower and upper Zaghra units represent the above mentioned unconformity. The included granitic clasts yielded ages between 650 and 640 Ma and are set in a matrix with zircon age populations at ca. 1000, 750 and 630 Ma. The zircons from the surrounding granites indicate an emplacement age between 622–605 Ma (Andresen et al., 2014). This indicates rather a distal provenance for the conglomerate detritus. Such an assumption is supported by the remarkable rounding of the conglomerate clasts. In addition, the geochemical characteristics of the lower Zaghra unit graywackes and the pelites are derived mostly from pre-existing sedimentary rocks. However, the conglomerates include minor clasts of dacites and semi-pelites of local derivation. In terms of tectonic setting, the $\text{K}_2\text{O}/\text{Na}_2\text{O}$ ratios of the Zaghra

graywackes range mostly between 0.5–1.2, similar to those in graywackes deposited at an Andean-type continental margin. The same conclusion is reached by using the $\text{K}_2\text{O}/\text{Na}_2\text{O}$ versus the SiO_2 plot of Roser and Korsch (1986) and the discrimination diagram of Bhatia (1983), where the graywackes plot in the ACM field and extend to the CIA field. The studied graywackes also show an intermediate proportion of quartz (15–65%) with rock fragments that infer, according to Crook (1974), a tectonic ACM.

The clastic sediments comprise mainly fluvial-alluvial sediments accumulated in intermontaine basins. The latter are commonly half-grabens or tilted fault blocks in which the clasts of the conglomerate beds accumulate near the border fault. Repetition of conglomeratic layers might reflect reactivation of fault movements.

5.3.3 Metamorphism

The lower Zaghra unit volcanic rocks were metamorphosed under greenschist facies conditions, and so should strictly be called meta-basaltic andesites, meta-andesites and meta-dacites. They contain characteristic greenschist facies minerals. However, the rocks were not pervasively recrystallized but retain the structures and textures of the original volcanics. These volcanics, interbedded tuffs and the sedimentary layers were subjected to regional, low-pressure metamorphism, which was the main foliation-forming event, defined by oriented amphibole, biotite and/or chloritized biotite, and related to

the early compressional deformation phase where the foliation is accompanied by oriented stretching defined by stretched quartz and lithic fragments.

The metabasaltic andesites and metadacites exhibit a mineral assemblage of plagioclase + biotite + epidote + chlorite ± opaques ± actinolite ± quartz, which is characteristic of greenschist facies. The mineral assemblage in the metagraywackes includes quartz + plagioclase + hornblende + biotite + epidote ± chlorite ± garnet indicating a garnet zone condition. The metapelites have a mineral assemblage: quartz + plagioclase + biotite ± chlorite ± muscovite ± epidote ± almandine, also indicating the garnet zone; the latter represents the transition between the greenschist and amphibolite facies conditions (Miyashiro, 1994). It should be noted that the metamorphic grade of the metavolcanics lags behind that of the associated metasedimentary rocks. While the volcanics attained only greenschist facies, the sediments indicate a greenschist–amphibolite transitional zone. This is expected because the sediments are highly reactive due to their favourable chemical and mineralogical composition, fine grain-size and low mechanical cohesion. The Zaghra metasedimentary rocks display similar REE patterns with amphibolite facies metapelites and metawackes (Ujike, 1984; Fig. 12)

More or less similar low-grade metamorphism of basaltic andesites and andesites was described by Khalaf (1999) from Gebel Dokhan in the Eastern Desert, indicating that the andesites suffered lower-middle greenschist facies metamorphism as recorded by biotite–actinolite–chlorite–epidote–albite–quartz–opaques–sphene assemblages.

Some of the samples from the lower Zaghra unit are incorporated in low-pressure thermal aureoles. Metadacites and metatuffs show decussate and granoblastic textures, respectively. In addition, the appearance of fine andalusite grains together with garnet porphyroblasts that have grown over a foliated matrix of biotite, muscovite, plagioclase, K-feldspar and quartz in the metapelites is due to contact metamorphism, which is related most probably to the outcropping of a younger quartz-diorite-granodiorite intrusion. The P-T conditions estimated for this contact metamorphism, using the plagioclase–amphibole geothermo-barometer of Plyusnina (1982), has been estimated to be 540°C and <2 kbar. The temperature was also determined as 580–586°C, using the plagioclase–amphibole thermometer of Holland and Blundy (1994) at the assumed pressure of 2 kbar. Using Schmidt's calibration (1992), the aluminium content in the amphibole gives an estimated pressure of <2 kbar for the thermal metamorphism.

5.3.4 Comparison with other volcano-sedimentary successions

The volcano-sedimentary succession of Wadi Zaghra displays marked similarities to successions from the Ferani, Kid and Rutig areas in terms of the lithologies of both volcanics and related sediments (El-Gaby et al., 1991, 2002; Moussa, 2003; Samuel et al., 2011; Be'eri-Shlevin et al., 2011). The conglomerates of the Wadi Zaghra lower unit yielded zircons with depositional ages

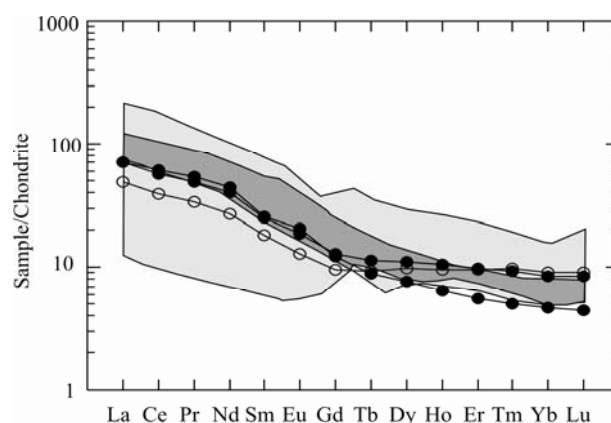


Fig. 12. Chondrite-normalized REE plots for the Zaghra meta-sedimentary rocks vs. amphibolite facies metapelites (dark gray) and metawackes (light gray); symbols as in Fig. 9.

of 625–615 Ma (Andresen et al., 2014), similar to those of the lower Rutig conglomerate that range between 620–610 Ma (Samuel et al., 2011). Moreover, the lower Rutig volcano-sedimentary section of ca. 630–615 Ma is unconformably overlain by the upper Rutig succession (615–590 Ma). Be'eri-Shlevin et al. (2011) and Moghazi et al. (2012) recorded ages for the volcano-sedimentary successions of Gebel Ferani and Wadi Kid of 607–593 Ma and 615–605 Ma, respectively. It is assumed, therefore, that the Ferani and Kid successions are comparable to the non-metamorphosed upper unit of the Zaghra succession. Both the Ferani and Kid successions, however, are metamorphosed in several localized contact thermal aureoles, caused mainly by concealed granitic intrusions. The new U-Pb age results for the Zaghra area given by Andresen et al. (2014), together with the present stratigraphic position and geochemical affinity, show that the Zaghra succession evolved coevally with the Dokhan Volcanics and Hammamat Clastics of the ED between 630 and 590 Ma (Wilde and Youssef, 2000; Breitreuz et al., 2010). The volcanic suite around Wadi Zaghra is enriched in most LILE and LREE and depleted in HFSE as well as HREE and exhibits subparallel fractionated REE patterns and normalized multi-element diagrams that are similar to those of the Dokhan Volcanics (Fig. 13).

The eruption of lower and upper volcanics around Wadi Zaghra was associated with the deposition of clastic sediments. Field investigation reveals that the volcanics occur within fault-bounded basins; the faults were documented by Shimron et al. (1993), Mehanna et al. (2001), El-Gaby et al. (2002) and Andresen et al. (2014). Also, the inclusion of sediments probably indicates the development of local basins. It is also possible that parts of the volcano-sedimentary succession developed over much wider areas and the present sequences are preserved patchy exposures (cf. Wilde and Youssef, 2001).

The tectonic environments of deposition of the Zaghra sediments fall mostly in the fields of ACM and CIA (Fig. 9c, d). The major elemental data of the Hammamat Clastics at Wadi Kid (El-Gaby et al., 1991; Sadek Ghabrial, 2000) and at the Wadi Hammamat type area (e.g. El Kalioubi, 1996; Holail and Moghazi, 1998; Abd El

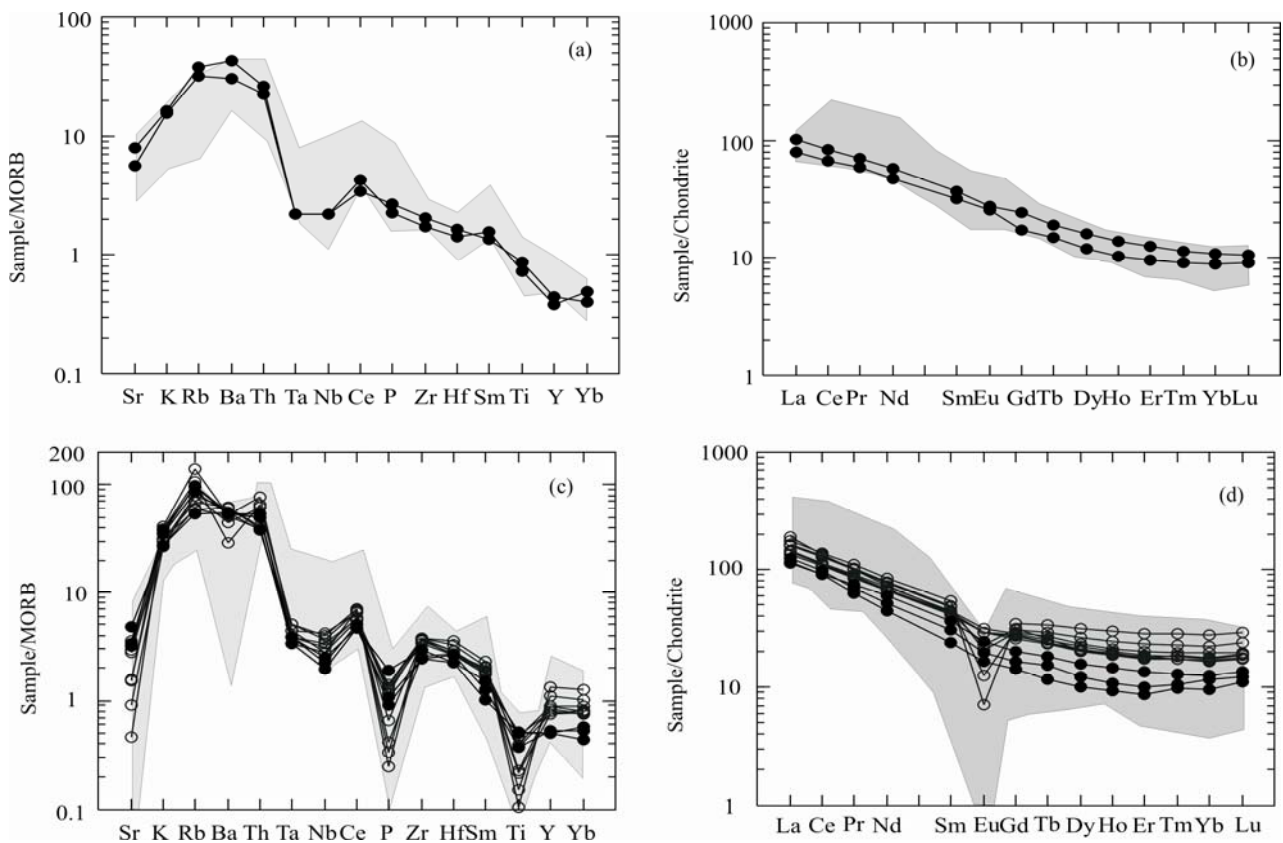


Fig. 13. (a) MORB normalized trace elements of the Zaghra basaltic andesite and andesite vs. Dokhan Volcanics of the E.D. of similar silica content; (b) Chondrite-normalized REE of the Zaghra basaltic andesite and andesite vs. Dokhan Volcanics of similar silica content; (c) MORB normalized trace elements of the Zaghra dacites and rhyolites vs. Dokhan Volcanics of similar silica content; (d) Chondrite-normalized REE of the Zaghra dacites and rhyolites vs. Dokhan Volcanics of similar silica content. Data sources are from Abdel Rahman (1996), Moghazi (2003), Eliwa et al. (2006); symbols as in Fig. 6.

-Rahman et al., 2010) are related to the same fields.

6 Conclusions

(1) The volcano-sedimentary succession around Wadi Zaghra, South Sinai includes intermediate to silicic volcanics of medium- to high-K calc-alkaline affinity, interbedded with rather immature sediments. The metamorphosed lower unit includes basaltic andesite, andesite and dacite associated with graywackes, semipelites and pelites. The lower unit is separated from the upper unit by thick (~20 m) metaconglomerates. The volcanics of the unmetamorphosed upper unit are dacites and rhyolites. The latter are highly fractionated and show A-type granite affinities, which may imply a change in the tectonic environment or that they were developed by extensive interaction of subduction-related magma with the continental crust. The associated sediments are litharenites, sublitharenites and minor arenites, i.e., more mature than lower unit sediments.

(2) The Zaghra volcanics as well as the Rutig, Ferani, Kid, Malhak and Iqna-Shar'a compare well in terms of geochemical patterns with the Dokhan Volcanics of the Eastern Desert. However, U-Pb dating (now in preparation) of the studied Zaghra volcanics is needed to confirm this correlation.

(3) The present geochemical data suggest that the Zaghra volcanic suite that ranges in composition from basaltic andesite to high-silica rhyolite is co-magmatic. It derived from a single intermediate calc-alkaline magma that erupted along an active continental margin. Contamination with the continental crust followed by fractional crystallization was responsible for the variation observed within this suite; plagioclase, amphibole and Fe-Ti oxides were the dominant fractionating phases. The associated clastics also suggest an active continental margin tectonic setting.

(4) Lithological traits, geochemical characteristics of the studied Zaghra succession together with LA-ICP-MS zircon ages from the remarkably rounded clasts of the metaconglomerates and their matrix together with the biotite schist and the surrounding intrusives reported by Andresen et al. (2014) negate the idea of proximal sources for the studied Zaghra sediments.

(5) Field relationship, metamorphic assemblage and whole-rock geochemistry suggest that the Zaghra volcano-sedimentary rocks are comparable to the Dokhan Volcanics and Hammamat Clastics of the ED. Thus, the Zaghra succession is not related either to the ensimatic island-arc assemblage or to the rift-related assemblage formed during the early stages of the break-up of Rodinia as previously thought.

Acknowledgements

Special thanks to Prof. Paul D. Asimow, California Institute of Technology, for his help with the microprobe analyses at Caltech. Also, the authors are grateful to Prof. E. El-Hinnawi, Professor of Mineralogy and Geochemistry, Earth Sciences Department, National Research Centre, Cairo, for critically reviewing the manuscript and for his comments and constructive remarks to improve it. Comments by the reviewers improved the present version of the manuscript. Dr Susan Turner and Dr. Fei Hongcai assisted with English.

Manuscript received Jul. 31, 2018
accepted Sept. 16, 2018
associate EIC YANG Jingsui
edited by TURNER Susan and FEI Hongcai

References

- Abdelfadil, K.M., Obeid, M.A., Azer, M.K., and Asimow, P.D., 2018. Late Neoproterozoic adakitic lavas in the Arabian-Nubian shield, Sinai Peninsula, Egypt. *Journal of Asian Earth Sciences*, 158: 301–323.
- Abdelsalam, M.G., and Stern, R.J., 1996. Sutures and Shear Zones in the Arabian-Nubian Shield. *Journal of African Earth Sciences*, 23: 289–310.
- Abdel Rahman, A.M., 1996. Pan-African volcanism: petrology and geochemistry of Dokhan volcanic suite in the northern Nubian Shield. *Geological Magazine*, 133: 17–31.
- Abd El-Rahman, Y., Polat, A., Fryer, B.J., Dilek, Y., El-Sharkawy, M., and Sakran, S., 2010. The provenance and tectonic setting of the Neoproterozoic Um Hassa Greywacke Member, Wadi Hammamat area, Egypt: Evidence from petrography and geochemistry. *Journal of African Earth Sciences*, 58: 185–196.
- Abu El-Ela, A.M., and El Bahariya, G.A., 1997. The Hammamat molasse sediments between Wadi Um Esh and Wadi Muweilih, Qift-Quseir Road Region, Central Eastern Desert, Egypt. *Egyptian Journal of Geology*, 41: 5–35.
- Agron, N., and Bendor, Y.K., 1981. The volcanic massif of Biq'at Hayareah (Sinai-Negev): A case of potassium metasomatism. *Journal of Geology*, 89: 479–495.
- Ali, K.A., Azer, M.K., Gahlan, H.A., Wilde, S.A., Samuel, M.D., and Stern, R.J., 2010. Age constraints on the formation and emplacement of Neoproterozoic ophiolites along the Allaqi-Heiani suture, South Eastern Desert of Egypt. *Gondwana Research*, 18: 583–595.
- Ali Bik, M.W., Abd El Rahim, S.H., Abdel Wahab, W., Abayazeed, S.D., Hassan, S.M., 2017. Geochemical constrains on the oldest arc rocks of the Arabian Nubian Shield: The late Mesoproterozoic to late Neoproterozoic (?) Sa'al volcano-sedimentary complex, Sinai, Egypt. *Lithos*, 284–285, 31–326.
- Andresen, A., Abu El-Enen, M.M., Stern, R.J., Wilde, S.A., and Ali, K.A., 2014. The Wadi Zaghra of Sinai, Egypt: new constraints on the late Cryogenian-Ediacaran tectonic evolution of the northernmost Arabian-Nubian Shield. *International Geology Review*, 56: 1020–1038.
- Azer, M.K., 2006. The petrogenesis of late Precambrian felsic alkaline magmatism in South Sinai, Egypt. *Acta Geologica Polonica*, 56: 463–484.
- Azer, M.K., 2007. Tectonic significance of Late Precambrian calc-alkaline and alkaline magmatism in Saint Katherina area, South Sinai Egypt. *Geologica Acta*, 5(3): 255–272.
- Azer, M.K., Obeid, M.A., and Ren, M., 2014. Geochemistry and petrogenesis of late Ediacaran (580-605 Ma) post-collisional alkaline rocks from Katherina Ring complex, south Sinai., Egypt. *Journal of Asian Earth Science*, 93: 229–252.
- Be'eri-Shlevin, Y., Katzir, Y., and Whitehouse, M., 2009. Post-collisional tectonomagmatic evolution in the northern Arabian-Nubian Shield (ANS): time constraints from ion-probe U-Pb dating of zircon. *Journal of the Geological Society*, London, 166: 71–85.
- Be'eri-Shlevin, Y., Eyal, M., Eyal, Y., Whitehouse, M.J., and Litvinovsky, B., 2012. The Sa'al volcano-sedimentary complex (Sinai, Egypt). A latest Mesoproterozoic volcanic arc in the northern Arabian Nubian Shield. *Geology*, 40: 403–406.
- Be'eri-Shlevin, Y., Samuel, M.D., Azer, M.K., and Rämö, O.T., Whitehouse, M.J., Moussa, H.E., 2011. The Ediacaran Ferani and Rutig volcano-sedimentary successions of the northernmost Arabian-Nubian Shield (ANS): New insights from zircon U-Pb geochronology, geochemistry and O-Nd isotope ratios. *Precambrian Research*, 188: 21–44.
- Bendor, Y.K., 1985. The crustal evolution of the Arabo-Nubian Massif with special reference to Sinai Peninsula. *Precambrian Research*, 28: 1–74.
- Bendor, Y.K., and Eyal, M., 1987. *The Geology of Sinai, its Implication for the Evolution of the Arabo-Nubian Massif, Jebel Sabbagh Sheet*. The Israel Academy of Sciences and Humanities, 484.
- Beyth, M., Stern, R., Altherr, R., and Kröner, A., 1994. The late Precambrian Timna igneous complex, Southern Israel: evidence for comagmatic-type sanukitoid monzodiorite and alkali granite magma. *Lithos*, 31: 103–124.
- Bhatia, M.R., 1983. Plate tectonics and geochemical composition of sandstones. *Journal of Geology*, 91: 611–627.
- Bhatia, M.R., 1985. Rare earth geochemistry of Australian Paleozoic greywackes and mudrocks: Provenance and tectonic control. *Sedimentary Geology*, 45: 97–113.
- Bhatia, M.R., and Crook, K.A.W., 1986. Trace element characteristics of greywackes and tectonic setting discrimination of sedimentary basins. *Contributions to Mineralogy and Petrology*, 92: 181–193.
- Breitreuz, C., Eliwa, H., Khalaf, I., El Gameel, K., Bühler, B., Sergeev, S., Larionov, A., and Murata, M., 2010. Neoproterozoic SHRIMP U-Pb zircon ages of silica-rich Dokhan Volcanics in the North Eastern Desert, Egypt. *Precambrian Research*, 182: 163–174.
- Campbell, F.A., and Williams, G.D., 1965. Chemical composition of shales of Mannville Group (Lower Cretaceous) of Central Alberta, Canada. *AAPG Bull.*, 49: 81–87.
- Condie, K.C., 1989. *Plate tectonics and crustal evolution* (3rd Edition). New York: Pergamon Press. 476 pp.
- Crook, K.A.W., 1974. Lithogenesis and geotectonics: the significance of the compositional variations in flysch arenites (greywackes). In: Dott, R.H., and Shaver, R.H. (eds.), *Modern and Ancient Geosynclinal Sedimentation* (vol. 19). SEPM Special Publication, 304–310.
- Deer, W.A., Howie, R.A., and Zussman, J., 1992. *An Introduction to the Rock-Forming Minerals* (2nd Edition). London: Longman Scientific and Technical, 696.
- Dorais, M.J., Wintsch, R.P., and Becker, H., 2001. The Massabesic gneiss complex, New Hampshire: A study of a portion of the Avalon Terrane. *American Journal of Science*, 301: 657–682.
- El-Bialy, M.Z., 2010. On the Pan-African transition of the Arabian-Nubian Shield from compression to extension: the post-collision Dokhan volcanic suite of Kid-Malhak region, Sinai, Egypt. *Gondwana Research*, 17: 26–43.
- El-Gaby, S., 1983. Architecture of the Egyptian basement complex. In: Ali Sadek (ed.), *Proc. 5th Conf. Basement Tectonics*, Cairo University, Cairo, 5: 1–8.
- El-Gaby, S., 2007. Integrated classification and evolution of the Neoproterozoic Pan-African belt in Egypt. In: Mustafa Youssef (ed), *The 5th International Conference on the Geology of Africa*, 143–154.
- El-Gaby, S., Khudier, A.A., Abdel Tawab, M., and Atalla, R.F., 1991. The metamorphosed volcano-sedimentary succession of Wadi Kid, southeastern Sinai, Egypt. *Annals of Geological Survey of Egypt*, XVII: 19–35.
- El-Gaby, S., Khalaf, I.M., Eliwa, H.A., El-Miligy, A., and Gomaa, R.M., 2002. The volcano-sedimentary successions of the Wadi Sa'al-Wadi Zaghra area, Southeastern Sinai Egypt. In: Ali Sadek (ed), *6th International Conference on Geological Arab World*, Cairo University, Egypt 1, 25–44.
- El-Gaby, S., List, F.K., and Tehrani, R., 1988. *Geology*,

- evolution and metallogenesis of the Pan-African belt in Egypt. In: El-Gaby, S., and Greiling, R. (eds.), *The Pan-African belt of NE Africa and adjacent areas*. Braunschweig, Wiesbaden: Vieweg, 17–68.
- Eliwa, H.A., Kimura, J.I., and Itaya, T., 2006. Late Neoproterozoic Dokhan volcanic rocks, northern Eastern Desert, Egypt. *Precambrian Research*, 151: 31–52.
- El Kalioubi, B., 1996. Provenance, tectonic setting and geochemical characteristics of the Hammamat molasse sediments around Um Had pluton, Eastern Desert, Egypt. *MERC Ain Shams University, Earth Science Series*, 10: 75–88.
- Ewart, A., 1982. The mineralogy and petrology of Tertiary-Recent Orogenic volcanic rocks with special reference to the andesitic-basaltic compositional range. In: Thorpe, R.S. (ed.), *Orogenic Andesites and Related Rocks*. Chichester: Wiley, 26–87.
- Eyal, M., and Hezkiyahu, T., 1980. Katharina pluton: the outline of a petrologic framework. *Israel Journal of Earth Science*, 29: 41–52.
- Eyal, M., Bartov, Y., Shimron, A.E., and Bentor, Y.K., 1980. *Sinai geological map, aeromagnetic map. Survey of Israel, Scale: 1:500 000, 1 sheet*.
- Eyal, M., Be'eri-Shlevin, Y., Eyal, Y., Whitehouse, M.J., and Litvinovsky, B., 2013. Three successive Proterozoic island arcs in the Northern Arabian-Nubian Shield: Evidence from SIMS U–Pb dating of zircon. *Gondwana Research*, 25: 338–357.
- Eyal, M., Litvinovsky, B., Jahn, B.M., Zanzvilevich, A., and Katzir, Y., 2010. Origin and evolution of post-collisional magmatism: Coeval Neoproterozoic calc-alkaline and alkaline suites of the Sinai Peninsula. *Chemical Geology*, 269: 153–179.
- Farahat, E.S., and Azer, M.K., 2011. Post-collisional magmatism in the northern Arabian-Nubian Shield: the geotectonic evolution of the alkaline suite at Gebel Tarbush area, south Sinai, Egypt. *Chemie der Erde*, 71: 247–266.
- Fowler, A., Hassen, I., and Hassan, M., 2015. Tectonic evolution and setting of the Sa'al Complex, southern Sinai, Egypt: A Proterozoic continental back-arc rift model. *Journal of African Earth Sciences*, 104: 103–131.
- Fritz-Töpfer, A., 1991. Geochemical characterization of Pan-African dyke swarms in southern Sinai: from continental margin to intraplate magmatism. *Precambrian Research*, 49: 281–300.
- Furnes, H., Shimron, A.E., and Roberts, D., 1985. Geochemistry of Pan African volcanic arc sequences in south eastern Sinai and plate tectonic implications. *Precambrian Research*, 29: 259–382.
- Garfunkel, Z., 1999. History and paleogeography during the Pan-African orogen to stable platform transition: reappraisal of the evidence from the Elat area and the northern Arabian-Nubian Shield. *Israel Journal of Earth Sciences*, 48: 135–157.
- Gorton, M.P., and Schandl, E.S., 2000. From continents to island arcs: A geochemical index of tectonic setting for arc-related and within-plate felsic to intermediate volcanic rocks. *The Canadian Mineralogist*, 38: 1065–1073.
- Grothaus, B., Eppler, D. and Ehrlich, R., 1979. Depositional environment and structural implications of the Hammamat Formation, Egypt. *Annals of the Geological Survey of Egypt*, IX: 564–590.
- Hassan, M., Abu-Alam, T.S., Stüwe, K., Fowler, A., and Hassen, I., 2014. Metamorphic evolution of the Sa'al-Zaghra Complex in Sinai: Evidence for Mesoproterozoic Rodinia break-up? *Precambrian Research*, 241: 104–128.
- Hawkesworth, C.J., Gallagher, K., Hergt, J.M., and McDermott, F., 1993. Mantle and slab contributions in arc magmas. *Annual Reviews of Earth and Planet Sciences* 21, 175–204.
- Hegazi, A.M., 2006. Tectonic evolution of the polydeformed Sa'al Belt, South Sinai, Egypt. *Acta Geologica Hungaria*, 49: 271–284.
- Holland, T.J.B., and Blundy, J.D., 1994. Non-ideal interactions in calcic amphiboles and their bearing on amphibole-plagioclase thermometry. *Contributions to Mineralogy and Petrology*, 116: 433–447.
- Holail, H.M., and Moghazi, A.M., 1998. Provenance, tectonic setting and geochemistry of greywackes and siltstones of the Late Precambrian, Hammamat Group, Egypt. *Sedimentary Geology*, 116: 227–250.
- Irvine, T.N., and Baragar, W.R.A., 1971. A guide to the chemical classification of the common volcanic rocks. *Canadian Journal of Earth Sciences*, 8: 523–548.
- Jarrar, G., Stern, R.J., Saffarini, G., and Al-Zubi, H., 2003. Late- and post-orogenic Neoproterozoic intrusions of Jordan: implications for crustal growth in the northernmost segment of the East African orogen. *Precambrian Research*, 123: 295–319.
- Johnson, P.R., Halverson, G.P., Kusky, T.M., Stern, R.J. and Pease, V. 2013. Volcanosedimentary Basins in the Arabian-Nubian Shield: Markers of Repeated Exhumation and Denudation in a Neoproterozoic Accretionary Orogen. *Geosciences*, 3(3): 389–445.
- Khalaf, E.E., 1999. Composition-volume changes during metasomatic alteration of Pan-African andesitic volcanic rocks at Gabal El Dokhan area, North Eastern Desert, Egypt. *JKAU: Earth Science*, 11: 177–206.
- Khalil, A.E.S., Obeid, M.A. and Azer, M.K., 2014. Serpentinized peridotites at the north part of Wadi Allaqi district (Egypt): Implications for the tectono-magmatic evolution of fore-arc crust. *Acta Geologica Sinica (English Edition)*, 88(5): 1421–1436.
- Le Maitre, R.W., 2002. *Igneous rocks: A classification and glossary of terms*. Second Edition. Cambridge: Cambridge University Press, 236.
- Leake, B.E., 1978. Nomenclature of amphiboles. *Mineralogical Magazine*, 42: 533–563.
- Leake B.E., 1997. Nomenclature of amphiboles: Report of the Subcommittee on Amphiboles of the International Mineralogical Association Commission on New Minerals and Mineral names. *Mineralogical Magazine*, 61: 295–321.
- Li, C., Tao, R., Huang, J., Han, R., Zhou, H. and Feng, Z., 2017. Geochemical characteristics of the Tayuan volcanic rocks in the Daxinganling metallogenic belt. *Acta Geologica Sinica (English Edition)*, 91(s1): 68–69.
- McLennan, S.M., 1989. Rare earth elements in sedimentary rocks: Influence of provenance and sedimentary processes. *Reviews in Mineralogy and Geochemistry*, 21: 169–200.
- McLennan, S.M., and Taylor, S.R., 1991. Sedimentary rocks and crustal evolution: tectonic setting and secular trends. *Journal of Geology*, 99: 1–22.
- Meert, J.G., 2003. A synopsis of events related to the assembly of eastern Gondwana. *Tectonophysics*, 362: 1–40.
- Mehanna, A.M., El Amawy, M.A., Wetait, M.A., and Soliman, F.A., 2001. Petrogenesis and structural synthesis of the metaconglomerates of Wadi Zaghra area: The base of metasediments in central south Sinai, Egypt. *Egyptian Journal of Geology*, 45: 11–36.
- Miyashiro, A., 1994. *Metamorphic petrology*. London: UCL Press, 404.
- Morimoto, N., 1988. Nomenclature of pyroxenes. *Mineralogical Magazine*, 52: 535–550.
- Moghazi, A.M., 2003. Geochemistry and petrogenesis of a high-K calc-alkaline Dokhan volcanic suite, south Safaga area, Egypt: the role of Late Neoproterozoic crustal extension. *Precambrian Research*, 125: 161–178.
- Moghazi, A.M., Ali, K.A., Wilde, S.A., Zhou, Q., Andresen, T., Andresen, A., Abu El-Enen, M.M., and Stern, R.J., 2012. Geochemistry, geochronology, and Sr–Nd isotopes of the Late Neoproterozoic Wadi Kid volcano-sedimentary rocks, southern Sinai, Egypt: implications for tectonic setting and crustal evolution. *Lithos*, 154: 147–165.
- Moussa, H.E., 2003. Geologic setting, petrography and geochemistry of the volcano-sedimentary succession at Gebel Ferani area, southeastern Sinai, Egypt. *Egyptian Journal of Geology*, 47: 153–173.
- Nachit, H., Ibhi, A., Abia, E., and Ohoud, M.B., 2005. Discrimination between primary magmatic biotites, reequilibrated biotites and neofomed biotites. *C.R. Geoscience*, 337: 1415–1420.
- Pearce, J.A., Harris, N.B.W., and Tindle, A.G., 1984. Trace element discrimination diagrams for the tectonic interpretation of granitic rocks. *Journal of Petrology*, 25: 956–983.
- Plyusnina, L.P., 1982. Geothermometry and geobarometry of plagioclase-hornblende bearing assemblages. *Contributions to Mineralogy and Petrology*, 80: 140–146.

- Potter, P.E., Shimp, N.F., and Witters, J., 1963. Trace elements in marine and fresh-water argillaceous sediments. *Geochimica et Cosmochimica Acta*, 27: 669–694.
- Richard, L.R., 1995. *Mineralogical and Petrological Data Processing System*. Minpet Software (c) 1988–1995, Version 2.02.
- Ries, A.C., Shackleton, R.M., Graham, R.H., and Fitches, W.R., 1983. Pan-African structures, ophiolites and mélanges in the Eastern Desert of Egypt: a traverse at 26°N. *Journal of the Geological Society of London*, 140: 75–95.
- Rittmann, A., 1962. *Volcanoes and their activity*. Place: Interscience Publishers, 395.
- Roser, B.P., and Korsch, R.J., 1986. Determination of tectonic setting of sandstone-mudstone suites using SiO₂ content and K₂O/Na₂O ratio. *Journal of Geology*, 94: 635–650.
- Roser, B.P., and Korsch, R.J., 1988. Provenance signatures of sandstone-mudstone suites determined using discriminant function analysis of major-element data. *Chemical Geology*, 67: 119–139.
- Roser, B.P., and Korsch, R.J., 1999. Geochemical characterization, evolution and source of a Mesozoic accretionary wedge: the Torlesse terrain, New Zealand. *Geological Magazine*, 136: 493–512.
- Rudnick, R.L., and Gao, S., 2003. Composition of the continental crust. In: Holland, H.D., and Turekian, K.K. (eds.), *Treatise of Geochemistry 3. The Crust*. Amsterdam: Elsevier, 1–64.
- Sadek Ghabrial, D., 2000. The Hammamat metasedimentary sequence in southeastern Wadi Kid area, south Sinai, Egypt. M.E.R.C. Ain Shams University, *Earth Sciences Series*, 14: 1–14.
- Samuel, M.D., Be'eri-Shlevin, Y., Azer, M.K., Whitehouse, M.J., and Moussa, H.E., 2011. Provenance of conglomerate clasts from the volcano-sedimentary sequence at Wadi Rutig in southern Sinai, Egypt as revealed by SIMS U–Pb dating of zircon. *Gondwana Research*, 20: 450–464.
- Samuel, M.D., Moussa, H.E., and Azer, M.K., 2001. Geochemistry and petrogenesis of Iqna Shar, a volcanic rocks Central Sinai, Egypt. *Egyptian Journal of Geology*, 45: 921–940.
- Samuel, M.D., Mousaa, H.E., and Azer, M.K., 2007. A-type volcanics in Central Eastern Sinai, Egypt. *Journal of African Earth Sciences*, 47: 203–226.
- Schmidt, M.W., 1992. Amphibole composition in tonalite as a function of pressure: An experimental calibration of the Al-in-hornblende barometer. *Contributions to Mineralogy and Petrology*, 110: 304–310.
- Schürmann, H.M.E., 1966. *The Precambrian along the Gulf of Suez and the Northern Part of the Red Sea*. Leiden: E. J. Brill, 404.
- Shimron, A.E., 1980. Proterozoic island arc volcanism and sedimentation in Sinai. *Precambrian Research*, 12: 437–458.
- Shimron, A., Bogoch, R., Furnes, H., and Roberts, D., 1993. The Sa'al Group: An ensialic island arc sequence in Sinai. In: Thorweihe, U., Schandelmeyer, H. (eds.), *Geoscientific research in northeast Africa*. Rotterdam: Balkema, 49–53.
- Stein, M., 2003. Tracing the plume material in the Arabian–Nubian Shield. *Precambrian Research*, 123: 223–234.
- Stern, R.J., 1994. Arc assembly and continental collision in the Neoproterozoic East African Orogen implications for the consolidation of Gondwanaland. *Annual Reviews of Earth Planetary Science*, 22: 319–351.
- Stern, R.J., and Gottfried, D., 1986. Petrogenesis of a Late-Precambrian (575–600 Ma) bimodal suite in northern Africa. *Contributions to Mineralogy and Petrology*, 92: 492–501.
- Stern, R.J., Gottfried, D., and Hedge, C.E., 1984. Late Precambrian rifting and crustal evolution in the Northeastern Desert of Egypt. *Geology*, 12: 168–172.
- Stern, R.J., Johnson, P.R., Kröner, A., and Yibas, B., 2004. Neoproterozoic ophiolites of the Arabian-Nubian Shield. In: Kusky, T.M. (ed.), *Precambrian Ophiolites and Related Rocks*. Developments in Precambrian Geology. Amsterdam: Elsevier, 13: 95–128.
- Stoeser, D.B., and Frost, C.D., 2006. Nd, Pb, Sr and O isotopic characterization of Saudi Arabian Shield terranes. *Chemical Geology*, 226: 163–188.
- Sylvester, P.J., 1989. Post-collisional alkaline granites. *Journal of Geology*, 97: 261–281.
- Takla, M.A., 2002. Economic potentialities of the Shield and Phanerozoic rocks of Egypt. In: Ali Sadek, (ed.), *6th International Conference of the Geology of Arab World*, Cairo University, March 2002, (Abstract, page16).
- Taylor, S.T., and McLennan, S.M., 1985. *The Continental Crust: its Composition and Evolution*. Oxford: Blackwell Science Publisher, 312.
- Ujike, O., 1984. Chemical composition of Archean Pontiac metasediments, southwestern Abitibi belt, Superior Province. *Canadian Journal of Earth Sciences*, 21: 727–731.
- Whalen, J.B., Currie, K.L., and Chappell, B.W., 1987. A-type granites: geochemical characteristics, discrimination and petrogenesis. *Contributions to Mineralogy and Petrology*, 95: 407–419.
- Wilson, M., 1994. *Igneous Petrogenesis*. London: Chapman and Hall, 466.
- Wilde, S.A., and Youssef, K., 2000. Significance of SHRIMP U–Pb dating of imperial porphyry and associated Dokhan Volcanics, Gebel Dokhan, North Eastern Desert, Egypt. *Journal of African Earth Sciences*, 31: 403–413.
- Wilde, S.A., and Youssef, K., 2001. SHRIMP U–Pb dating of detrital zircons from Hammamat Group at Gebel Um Tawat, Northern-Eastern Desert, Egypt. *Gondwana Research*, 4: 202–206.
- Wimmenauer, W., 1984. Das Praevariszische Kristallin im Schwarzwald. *Fortschritte der Mineralogie*, 62: 69–86.
- Zuochen, L., Xianzhi, P., Ruibao, L., Lei, P., Chengjun, L., Youxin, C., Tong, X., Jie, Y. and Bo, W., 2015. U–Pb zircon geochronology and geochemistry of the Neoproterozoic Liujiaping Group volcanics in the northwest margin of the Yangtze Block: Implications for the breakup of the Rodinia supercontinent. *Acta Geologica Sinica (English Edition)*, 89 (4): 1213–1225.

About the first author



Prof. Mekhaiel D. SAMUEL was born in Sohag, Egypt in 1939. He is Research Professor of Petrology and Mineralogy at National Research Centre, Egypt. Graduated from Ain Shams University in 1959, with B.Sc. in Geology and Chemistry. Awarded M.Sc. in Geology from Ain Shams University and Ph.D., in Geology from Cairo University in 1965 and 1970, respectively.

About the corresponding author



Mokhles, K. AZER is a professor of geological sciences who specializes in igneous and metamorphic petrology and regional tectonics, with a particular research focus on the petrogenesis and geochemistry of juvenile crust of the Arabian-Nubian Shield exposed in Eastern Desert and Sinai. He was born in Assiut, Egypt in 1972.

Graduated his M.Sc. and PhD from Cairo University in 2000 and 2004, respectively. Dr. Azer worked in many intentional projects in cooperation with different foreign countries as principle investigator, co-principal investigator and as a member. Also, he awarded many prizes due to his outstanding contributions to the geology of Egypt. Many local and international workshops are organized by Prof. Azer to correlate the geology of Egypt, especially the Red Sea region, with those of other countries. Now he holds the position of Head of Geological Sciences Department at the National Research Center, Egypt.